9 Light scattering in combustion

Alan R. Jones

9.1 Introduction

Combustion very often involves two-phase flow. This takes the form of a gas containing fuel and/or combustion products. Mostly, the fuel is either a liquid spray or pulverised coal, though other solids may be present such as biological waste (biomass) and even sewerage. The products are very commonly soot, but also ash and char. Flames are also used in the manufacture of particles such as carbon black and pigments, and recently there has been growing interest in the production of nanoparticles.

In research to understand combustion processes and in industry to monitor combustor performance it is necessary to be able to measure the rates of conversion of the fuel and of formation of the products. The mass flow rate of particulate matter is also an important consideration, both in performance and in emissions control.

Flames and combustion products are very hostile environments. The temperatures involved are normally well in excess of 1000°C. This, combined with the high flow rates and bombardment by particles, is damaging to any probes that are inserted into the gas stream. This is one of the reasons why optical techniques have been developed into powerful tools for combustion diagnostics. Apart from the windows necessary in some cases, all the optical components are external to the combustion system. In addition, electromagnetic radiation at moderate intensities does not significantly interfere with the object under study, unlike, for example, the insertion of a probe.

The interaction of radiation with solid particles or liquid drops is covered under the generic term 'scattering'. The nature of the interaction depends upon the particle size, shape, structure, concentration and refractive index. In principle, therefore, scattering can be used to measure all of these variables. The nature of the scattering process can be a simple rebound not involving a change in frequency, other than Doppler shift. This is elastic scattering. Alternatively, there may be frequency shifts due to absorption and re-emission or due to nonlinear effects. This is inelastic scattering. This chapter will be restricted to elastic scattering and recent developments in this area will be reviewed.

Although the environment cannot damage a beam of light, there are some considerations when applying optics to combustion systems. The light will interact with the gas. In most cases, for the gases typically found in combustion systems and for visible wavelengths, it is the temperature gradients that are problematic because they cause deflections of the light that may lead to uncertainty in the position and size of the measurement space and spreading of the incident beam. There may also be a loss of intensity due to scattering out of the beam before it reaches the measurement point. A further difficulty in industrial combustors is that access may be limited and often only one port is available. Fogging of windows is also an important problem that will affect transmission of the light in and out of the combustor, leading not only to a loss of intensity but also to false results. For this reason, methods that do not rely on absolute intensity are to be preferred. Another problem is the presence of thermal radiation. This occurs at all wavelengths and can create difficulty in separating out the scattered signal.

Radiative emission from flames is influenced by scattering, and the presence of particulates can control heat transfer. The emission of radiation by particles can also be employed to measure temperature, common methods being total radiation and optical pyrometry and multi-colour methods. However, radiative emission is beyond the scope of this chapter. Further information can be found, for example, in Hottel and Sarofim (1967) and Modest (2003).

The emphasis here is to review recent work on the use of light scattering for diagnostics of particles relevant to flames and combustion. The author has written two earlier reviews (Jones, 1993, 1999) to which the reader is referred. This chapter will concentrate on developments since 1999. Reference to earlier work will be made only where necessary for reasons of clarity. In addition the review will concentrate on developments in techniques, and will not discuss results unless they are of a particularly fundamental nature.

9.2 Soot and other nanoparticles

When small particles formed in flames, such as soot, are sampled and viewed under an electron microscope they usually appear as branched chain agglomerates. Examples can be seen in Fig. 9.1. The aggregate is made up of a number of primary particles. For soot, the size of the primary particles is typically of the order 30–60 nm and the aggregates are up to 500 nm. The properties of the aggregates that we would like to measure include the sizes of the primary particles and the aggregates, both as functions of size and position. We would also like to follow the formation of the primary particles and the aggregation process, ultimately leading to smoke formation.

Apart from soot a number of other small particle types can be formed in flames. There is now a growing interest in the manufacture and uses of nanoparticles, and flames are a common source (Pratsinis, 1998; Wooldridge, 1998)

Before we can analyse the results of experimental measurements we need a theoretical basis to describe the scattering process. The importance of correctly

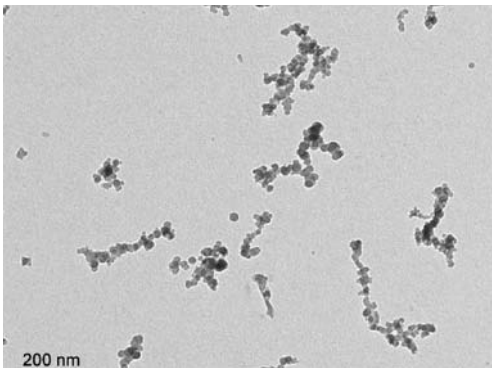

(a)

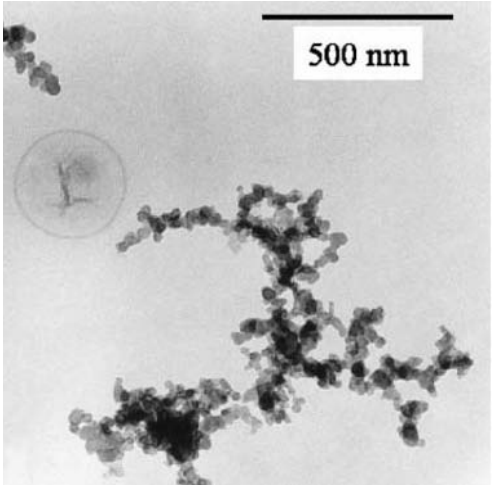

(b)

Fig. 9.1. Typical examples of soot aggregates sampled from flames. (a) Taken from Tian *et al.* (2004). (b) Taken from Wentzel *et al.* (2003).

treating aggregates has been demonstrated by Quinten *et al.* (2001). They compared scattering by aggregates with that of equal volume spheres in optical particle counters, which infer particle size from a measurement of scattered intensity. They demonstrated that scattered intensity increases due to irregularity caused by agglomeration. Models based on equal volume spheres with a variety of effective medium approximations failed to represent the experimental results.

In the case of aggregates of small particles there are two fundamental approaches. The first of these is full interactive scattering. Here there is a rigorous

theory (e.g. Xu, 1997; Xu and Gustafson, 2001; Saija *et al.*, 2003), but it is very complicated and very computer-intensive.

Because the monomers are so small they can be treated as Rayleigh scatterers and this leads to the coupled dipole method (e.g. Purcell and Pennypacker, 1973; Mulholland and Mountain, 1999; Xu and Gustafson, 1999; Shu and Charalampopoulos, 2000a). This is less complicated, but still involves the solution of $3N$ simultaneous equations, where N is the number of monomers in the aggregate. The advantage of the rigorous theories is that they will predict polarisation properties of the aggregates, as well as being accurate. The main disadvantage is that the position of every particle must be known. This is not possible even for one agglomerate, let alone a group of aggregates. Theorists get around this problem by simulating the aggregation process so that the positions are known.

A simpler approach arises from the observation that the aggregates are usually tenuous by nature. This leads to the prospect that the incident wave may propagate undisturbed through the structure, and that the Rayleigh–Gans–Debye (RGD) approximation may be applied. Where this is suitable the primary particles may be considered to scatter independently. The resulting analysis is then much more straightforward.

The positions of the primary particles cannot be predicted in any one aggregate, and all aggregates are different from each other. Overall the positions may be considered to be random. This suggests a statistical method, which leads to the concept of a correlation function. This is quite easily applied in the RGD model using the fractal approach; the so-called Rayleigh–Gans–Debye–fractal-aggregate (RGD-FA) model. Excellent reviews of this method have been given by Sorensen (2001) and Bushell *et al.* (2002).

Wang and Sorensen (2002) found good agreement between RGD theory and experiment for fractal aggregates. The materials used were TiO_2 ($m = 2.61$) and SiO_2 ($m = 1.46$). The primary particle size was of the order of 20 nm with about 150 per cluster. Van-Hulle *et al.* (2002a) examined the validity of the RGD-FA approach by comparison of theoretical results from the rigorous multisphere model using translation vectors (Xu, 1997) and the coupled dipole method. For scattering at 90° the two approximations were in reasonable agreement but disagreed with the rigorous solution. All three were in good agreement for the absorption and extinction coefficients, but RGD-FA was low for the scattering cross-section. di Stasio (2002b) has also queried whether the RGD-FA method obeys the optical theorem. Evidently these questions require further study.

In the RGD method the scattering is described in terms of the scattering wave vector $\boldsymbol{q}$, which has the magnitude

$$q = \frac{4\pi}{\lambda} \sin \frac{\theta}{2}$$

where θ is the angle between the incident and scattered directions. For a set of N scatterers the intensity becomes

$$I(q) = \left| \sum_{n=1}^{N} \mathrm{e}^{i\boldsymbol{q}\cdot\boldsymbol{r}_n} \right|^2 = \sum_{n=1}^{N} \sum_{m=1}^{N} \mathrm{e}^{i\boldsymbol{q}\cdot(\boldsymbol{r}_n - \boldsymbol{r}_m)}$$

where $\boldsymbol{r}_n$ is the position of the nth particle. This may also be written

$$I(q) = F(q)S(q)$$

where $F(q)$ describes the scattering by individual particles and $S(q)$ is the structure function. For N independent Rayleigh particles $F(q) \propto N^2$ and so

$$S(q) \propto \frac{1}{N^2} \sum_{n=1}^{N} \sum_{m=1}^{N} \mathrm{e}^{i\boldsymbol{q}\cdot(\boldsymbol{r}_n - \boldsymbol{r}_m)}$$

A powerful method of overcoming the lack of knowledge of the positions of the individual particles is to describe the agglomerates as fractal structures. These are defined by

$$N = K \left(\frac{R_\mathrm{g}}{a_\mathrm{p}} \right)^{D_\mathrm{f}}$$

where R_g is the radius of gyration, a_p is the radius of the primary particles and N is the number of primary particles in the agglomerate. K is a constant prefactor and D_f is the dimension. For infinite cylinders $D_\mathrm{f} = 1$, for flat discs $D_\mathrm{f} = 2$ and for spheres $D_\mathrm{f} = 3$. However, for these structures D_f is not found to be an integer, rather it is some fraction; hence the term 'fractal dimension'. For a soot agglomerate D_f is typically about 1.8.

The RGD approximation works reasonably well for $D_\mathrm{f} < 2$. For $D_\mathrm{f} > 2$ the agglomerate is too dense and the aggregate is better described by rigorous theory. As D_f approaches 3, Mie theory may be used.

It is worth noting here that the agglomerate is not a genuine fractal. For that, the properties should be independent of scale. Clearly, this is not so for the aggregate. If the scale is very small then individual primary particles play the most significant role. If the scale is very large it can be outside the limits of the actual aggregate. The correlation function has to be multiplied by a cut-off function to allow for this. Sorensen (2001) discusses this theory in detail.

The outcome of the analysis is that there are three regimes:

1. The Guinier regime ($qR_\mathrm{g} \ll 1$) where scattering is dominated by the large scale of the agglomerate. Here

$$S(q) = 1 - \frac{1}{3}(qR_\mathrm{g})^2$$

   A plot of $I(q)$ against q^2 will yield the radius of gyration.
2. The power law regime ($qR_\mathrm{g} \gg 1$) where interactive scattering and the structure of the agglomerate are important. Here

$$S(q) \propto (qR_\mathrm{g})^{-D_\mathrm{f}}$$

   A plot of $\ln[I(q)]$ against q will yield the fractal dimension.

3. For extremely large values of qR_g there is a third regime, sometimes known as the Porod regime, where scattering is dominated by the individual Rayleigh sized primary particles. Here

$$S(q) \propto q^{-4}$$

Thus, we can see that the measurement of scattered intensity against angle can yield both the radius of gyration of the agglomerate and the fractal dimension.

Fig. 9.2 shows the variation of these for soot as a function of height in a flame as measured by di Stasio (2001) and di Stasio *et al.* (2002). It can be seen that initially R_g is small and D_f is large, about 25 nm and 2.55 respectively. This is the region where the primary particles are either still separate or in the very early stages of agglomeration. Since for a sphere $D_f = 3$, we would expect a high value here. As agglomeration progresses R_g increases and D_f becomes smaller, eventually arriving at about 380 nm for R_g and 1.2 for D_f. In this case the agglomerates are similar to straight chains, as in Fig. 9.1(a). However, the agglomerate then begins to change shape. R_g falls to about 160 nm before further growth occurs taking it up to approximately 280 nm. At the same time the fractal dimension rises to almost 1.9. At this stage the agglomerate resembles that seen in Fig. 9.1(b). The reason for this restructuring is not clear, but the possibilities are discussed by the authors. Sorensen *et al.* (2003) and Kim *et al.* (2004) point to the possible formation of super-aggregates with fractal dimension as high as 2.6. They speculate that these may be formed by percolation of smaller aggregates with fractal dimension of 1.8, or by restructuring due to tenuous agglomerates subjected to shear flow.

Close to the burner it would be expected that individual soot monomers would form, and it would be of interest to detect the actual onset of agglomeration. A possible technique has been suggested by di Stasio (2002b) who claims that reciprocity is violated for very small agglomerates of about two particles. The author shows results that imply that at a certain height above the burner the ratio of cross-polarised intensities (I_{HV}/I_{VH}) can rise as high as six at a scattering angle of 120°. Higher up the burner, where the agglomerates are larger, the ratio returns to one and reciprocity is satisfied. However, reciprocity is such a well-established principle that the proposal should be treated with some caution[1].

Of course, the numbers suggested by Fig. 9.2 are not universal. The sizes and residence times will depend to some extent upon the fuel and the nature of the burner. However, the variation in size is not large and the fractal dimension is found to be reasonably universal. Also, the same kind of variation is found in the manufacture of other nanoparticles. As an example Fig. 9.3 shows results for

[1]It is worth noting that for larger agglomerates Shu and Charalampopoulos (2000a) state that previously reported violations of reciprocity arise from inappropriate orientation averaging. It is not sufficient to average only over angular orientations of the aggregate, but rotation about the axis must also be taken into account.

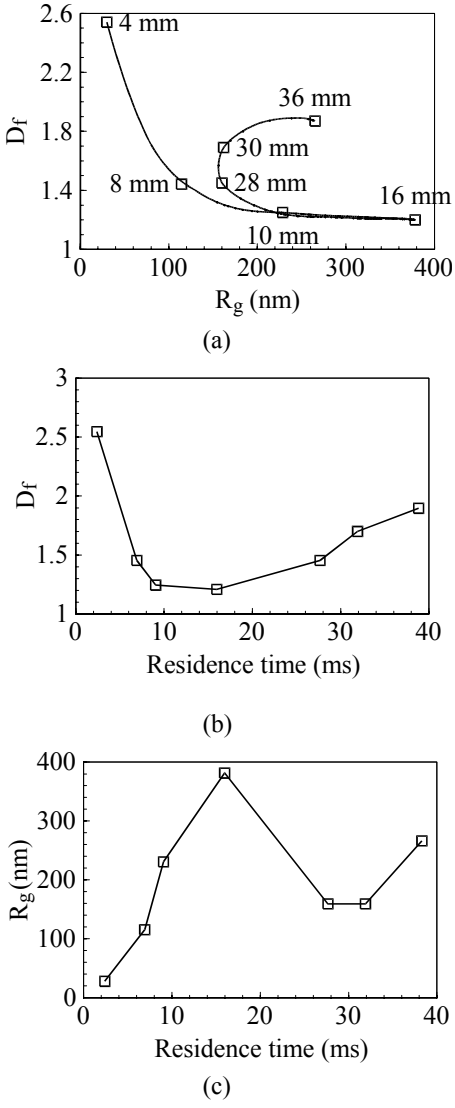

Fig. 9.2. Variation of radius of gyration and fractal dimension with (a) height in a flame (after di Stasio, 2001) and (b) and (c) residence time (after di Stasio *et al.* (2002a).

aluminium oxide formed in a flame obtained by Xing *et al.* (1999). In contrast to this, Kim and Choi (2003) found no evidence of rearrangement or sintering for silica particles formed in a flame.

It will be noted that the measurement of R_g and D_f is not a complete description of the aggregate. For this the size of the primary particles is needed and the number of particles in the aggregate. These could either be measured

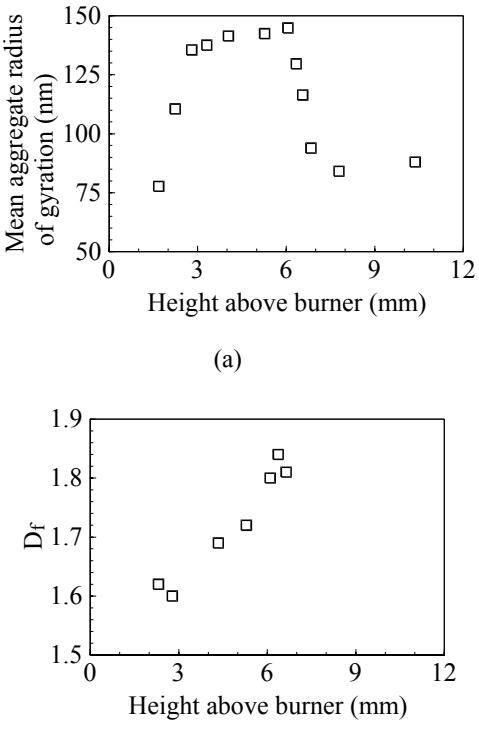

Fig. 9.3. Variation of the radius of gyration and fractal dimension for Al_2O_3 formed in a flame as a function of height above the burner (after Xing *et al.*, 1999).

independently, or one could be deduced from the other if the prefactor were known. Hu *et al.* (2003) used a combination of electron microscopy and laser extinction techniques and obtained $D_f = 1.74 \pm 0.11$ and $K = 2.2 \pm 0.4$. Brasil *et al.* (2000) commented that the fractal dimension is reasonably well understood with quoted values between 1.4 and 1.86, but that the prefactor can vary widely with quoted values between 1.05 and 3.5. They made an analysis with simulated aggregates with refractive indices typical of soot and alumina, which suggested a conclusive result. They found a fractal dimension of 1.82 and a prefactor of 1.27 independently of aggregate size and composition. However, they noted that experiments have yielded a dimension greater than 2. They suggested that this might be due in part to sintering and to polydispersity of the monomers.

Mulholland and Mountain (1999) performed calculations using a coupled electric and magnetic dipoles method, and concluded that there is a correlation between polarisation ratio

$$P = \frac{I_{\mathrm{HH}}(90^\circ)}{I_{\mathrm{VV}}(90^\circ)}$$

and the size of the primary particles. For a fixed number of particles in the agglomerate, their result is shown is shown in Fig. 9.4. It can be seen that there is an increasing trend, which for a point detector is linear. As the receiving aperture increases the linearity is corrupted. Krishnan *et al.* (2001) showed results for a range of measurements of polarisation ratio against primary particle size, as seen in Fig. 9.5. Again there is an increasing trend. In addition it will be observed that the ratios are higher for overfire soot with 260–552 particles per agglomerate than for underfire soot with 30–80 particles. This can be interpreted with aid of Fig. 9.6, taken from Mulholland and Mountain (1999). The polarisation ratio is predicted to increase or decrease with increasing number of particles depending upon the value of x_p. For small particles with $x_p < 0.2$ there is, indeed, a tendency to decrease.

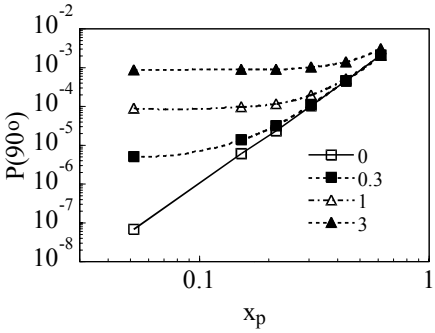

Fig. 9.4. Polarisation ratio versus size parameter of primary spheres for a range of detector acceptance angles in degrees (after Mulholland and Mountain, 1999).

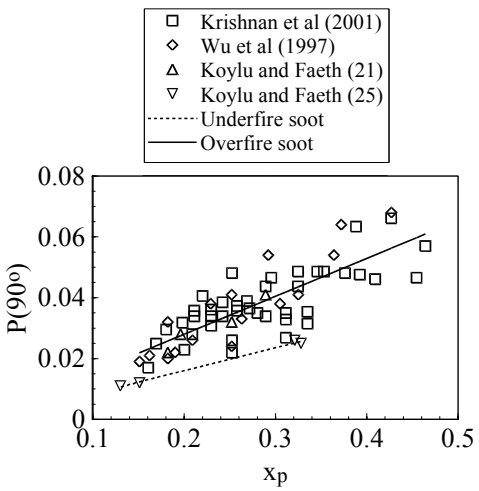

Fig. 9.5. Measurements of the polarisation ratio for various fuels as a function of the size parameter of the primary spheres (after Krishnan *et al.*, 2001).

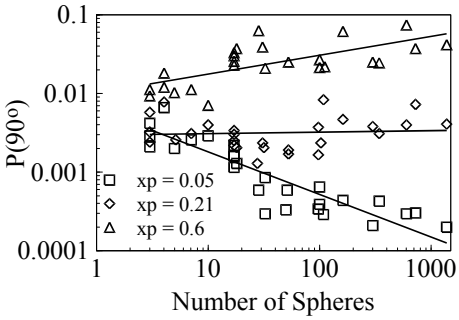

Fig. 9.6. Effects of primary size parameter and number of spheres in an agglomerate on the polarisation ratio for a detector acceptance angle of 2° (after Mulholland and Mountain, 1999).

Two methods for obtaining the primary particle size were proposed by di Stasio (2000). The first was also a linear relationship between the polarisation ratio and the primary particle size. This is illustrated in Fig. 9.7, but it is apparent that the negative gradient is in disagreement with the results presented in Fig. 9.5. The reason for this is again lies in the fact that the number of particles in the agglomerates and the primary particle size were both increasing with time.

Since for an isolated Rayleigh sized sphere I_{VV} is independent of angle; the angular variation is due to the structure function $S(q)$. The Fourier transform of the scattering pattern of I_{VV} is then the auto-correlation function, $G(r)$, of the aggregate structure. di Stasio's (2000) second method was to note that in the Porod regime the first peak in $G(r)$ corresponded to the primary particle diameter. The second peak corresponded to twice this diameter. An example of this function as measured by di Stasio (2000) is seen in Fig. 9.8. This technique has the advantage that the positions of the peaks are independent of the num-

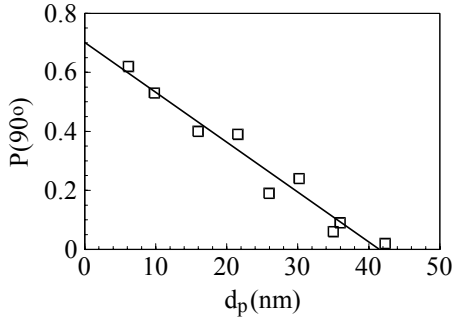

Fig. 9.7. Measured polarisation ratio versus primary particle size as obtained by scanning electron microscopy at corresponding heights above a Bunsen burner in an ethylene–air diffusion flame (after di Stasio, 2000).

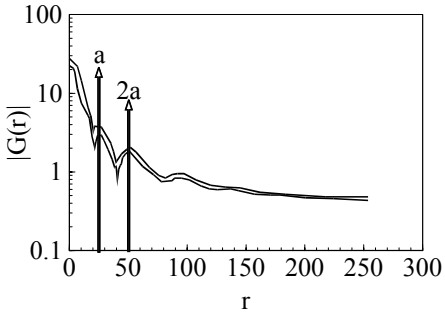

Fig. 9.8. Example of a density-density function $|G(r)|$ of fractal soot aggregates obtained by Fourier transformation of the measured structure function $S(q)$. The two lines represent the upper and lower envelopes of a rapidly oscillating curve (after di Stasio, 2000).

ber of particles, though that does affect the ratio of their heights. The author makes the point that the method may be limited by the need to ensure that q is sufficiently large (wavelength is sufficiently small) to ensure that the Porod regime is achieved.

Mulholland and Mountain (1999) suggested that the number of particles in an agglomerate could be obtained from the extinction cross-section provided that the primary particle size is known. di Stasio *et al.* (2002a) was able to infer this number from a measurement of the ratio of scattered intensities at 20° and 90°.

Krishnan *et al.* (2000, 2001) made measurements on sooting flames from both gaseous and liquid fuels. They based their analysis on RGD-FA but assumed a prefactor of 8.5, which is probably too high. Nonetheless, the fractal dimension was universally approximately 1.8 in general agreement with other authors. Some of their results are summarised in Table 9.1. From measurements of both

Table 9.1. A summary of some structure properties of overfire soot agglomerates (after Krishnan *et al.*, 2000).

Fuel	d_p (nm)	$\overline{N}$	D_f
Gas fuelled flames:			
Acetylene	47	417	1.79
Ethylene	32	467	1.80
Propylene	41	460	1.79
Butadiene	42	—	1.79
Liquid fuelled flames:			
Benzene	50	552	1.77
Cyclohexane	37	—	1.80
Toluene	51	526	1.79
n-Heptane	35	260	1.79

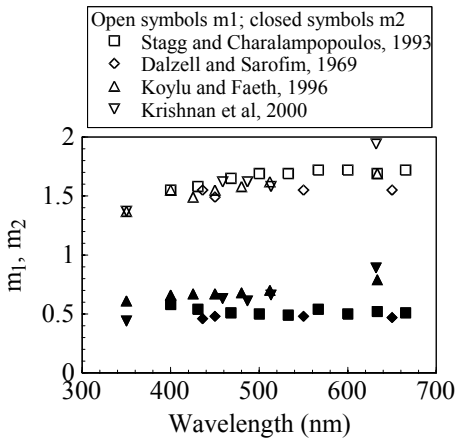

Fig. 9.9. Measurements of the real (m_1) and imaginary (m_2) parts of the refractive index of soot as reported by Krishnan *et al.* (2000).

scattered intensity and extinction coefficient they were able to determine both the functions

$$F(m) = \left|\frac{m^2-1}{m^2+2}\right|^2 \quad \text{and} \quad E(m) = \text{Im}\left(\frac{m^2-1}{m^2+2}\right)$$

so that in principle both the real and imaginary parts of the refractive index, m, could be established. The refractive index function for absorption $E(m)$ agreed with previous authors, but the scattering function $F(m)$ only agreed up to 550 nm, but then rose faster. Their results for refractive index are seen in Fig. 9.9. The measured values vary between approximately 1.4–i0.4 at 350 nm wavelength and 2–i0.9 at 660 nm.

Van-Hulle *et al.* (2002b) examined soot refractive index in turbulent methane flames with either air or oxygen. Soot sizes were obtained from sampling and then RGD theory applied to calculate the optical properties of fractal aggregates for comparison with measurement. Both extinction and $I_{\text{VV}}(90°)$ were measured at a wavelength of 632.8 nm and an inversion technique used to find the complex refractive index. Within experimental error the refractive index was independent of oxidiser and height above the burner and was 2–i0.5. Changing the morphological parameters was found to have important consequences on the predicted refractive index. A sensitivity analysis found that the fractal dimension is the most important variable overall, whereas d_{p} and K only influence the imaginary part. Their results are in reasonable agreement with the calculated value of 1.9–i0.55 of Lee and Tien (1981) and of the reflectance technique of 1.94–i0.64 of Mullins and Williams (1987). They also agree with the real part of 1.99–i0.89 given by Krishnan *et al.* (2000) but not with the imaginary part.

It is worth pointing out that the actual refractive index of soot is a function of a number of parameters. It will vary with carbon to hydrogen ratio in the soot, and this will depend upon the original fuel and oxidant combination and the age

of the soot in the flame. Examples of the variation that may be expected occur in the work of Charalampopoulos *et al.* (1989), Chang and Charalampopoulos (1990) and Vaglieco *et al.* (1990).

Charalampopoulos and Shu (2003) made experimental measurements on the fractal aggregates of Fe_2O_3 formed in a CO–air diffusion flame. Scattering, extinction and asymmetry were used and the measurements were combined with an exact light-scattering theory to yield the complex refractive index, the primary particle size parameter, the aspect ratio, and the number density and volume fractions of the chainlike aggregates under flame conditions. The effective complex refractive index was 1.96–i0.2. The corresponding primary particle size was found to be 48 nm and the aggregate aspect ratio was in the range of 6–7. The authors also provided an interesting discussion of the inversion procedure used to obtain the required data.

Apart from the variation of scattered intensity with angle, the other important variables are the scattering and extinction cross-sections. This is partly because they can indicate the absolute scattered intensity and because of the commonly used sizing method based on spectral extinction. In addition, however, the cross-sections are important to radiative heat transfer calculations. The optical properties of smoke are also critical to visibility and the design of escape routes and appropriate emergency lighting. Snegirev *et al.* (2001) were interested in the response of light scattering smoke detectors, and concluded that neglecting coagulation underestimated their response times. An example of the influence of fractal dimension on extinction is shown in Fig. 9.10. This indicates that the well-known peak in specific cross-section for spheres is not present for fractal agglomerates, and that the extinction increases with fractal dimension.[2] For a range of gaseous and liquid fuels, Krishnan *et al.* (2000) measured the dimensionless extinction coefficient defined by

$$\kappa_{\text{ext}} = -\lambda \ln(I/I_0)/(Lf_{\text{v}})$$

in the overfire region of flames and found it to be 8.5 almost independently of wavelength. However, Zhu *et al.* (2000) measured the dimensionless extinction coefficient at two wavelengths for soot from acetylene and ethene. For acetylene at a wavelength of 632.8 nm they found 8.1 and at 856 nm they obtained 8.8. The equivalent values for ethene were 9.7 and 9.4. For JP-8 soot Zhu *et al.* (2004) obtained values in the range 9.8 to 10.0 in the wavelength range 633 to 1565 nm. Widmann *et al.* (2003) demonstrated that the dimensionless extinction coefficient also depends on the fuel/air ratio, as seen in Fig. 9.11. It is worth noting that for most of these reports error values of at least ±0.5 were given.

[2]There is no evidence to doubt this calculation. However, it is slightly worrying that for fractal dimensions greater than 2 fractal theory may not be applicable (Berry and Percival, 1986; Farias *et al.*, 1995, 1996) and it is suggested that Mie theory may be appropriate. In Fig. 9.10 all the fractal calculations are higher than the Mie theory result and are increasing with fractal dimension. In support, it is noted that the Mie theory was applied to a volume equivalent sphere (not an actual sphere), and that the results are broadly in agreement with those of Dobbins *et al.* (1994).

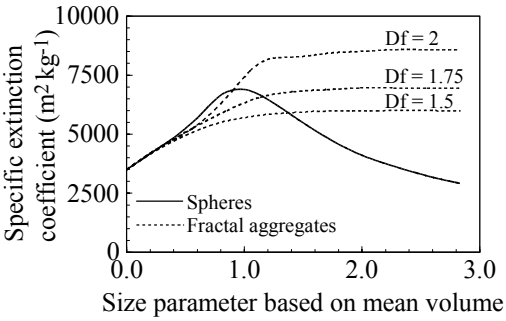

Fig. 9.10. Calculated specific extinction coefficient as a function of fractal dimension (after Snegirev *et al.*, 2001.

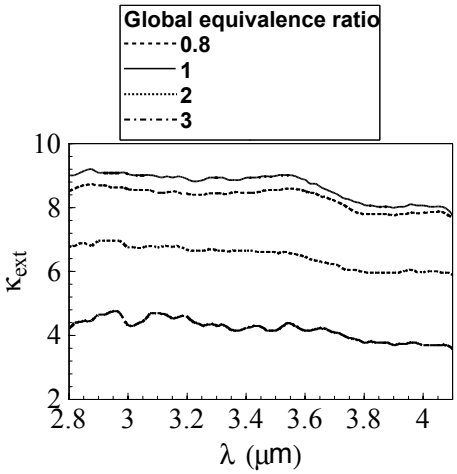

Fig. 9.11. Dimensionless extinction coefficient of soot agglomerates as a function of global equivalence ratio (after Widmann *et al.*, 2003). Only the mean curves are shown here; there is a variation of up to ±0.5 shown in the original. The sequence top to bottom is 1.0, 0.8, 2.0 and 3.0.

Mulholland and Croarkin (2000) quoted the mass specific extinction coefficient, which is given by

$$K_{\mathrm{m}} = -\ln(I/I_0)/(L\rho f_{\mathrm{v}})$$

to be $8.8 \pm 1.1\,\mathrm{m}^2\,\mathrm{g}^{-1}$ when averaged over 29 soots. Their interest was in fire research, and they commented that this nearly universal value means that the mass concentration of smoke can be inferred from extinction measurements. Mulholland *et al.* (2000) have described the design of a smoke concentration meter based on these principles.

Detailed calculations using a rigorous numerical method have been undertaken for fractal aggregates of soot by Klusek *et al.* (2003). Model clusters were derived to suit a chosen fractal dimension and extensive calculations of the scat-

tering matrix were performed. It was found that S_{12} and S_{34} are more sensitive to fractal properties than S_{11}. Detailed calculations were also discussed by Riefler *et al.* (2004) who used the T-matrix method. Models clusters were averaged both over orientation and over different clusters (configurational averaging). It was concluded that configurational averaging generally gives a superior fit to the measurements. They also emphasised that, while the T-matrix method is exact and superior to the RGD approach, it is much more consuming of time and effort.

Menguc and Manickavasagam (1998) also performed detailed calculations on simulated fractal aggregates. They investigated all the elements of the scattering matrix for soot with $D_\mathrm{f} = 1.8$, but with a prefactor of 5.8 which is rather large. They observed various interesting features of the various elements, and suggested that inversion procedures may be developed based on a library of calculated values. In particular they note that N and dp may be obtained from the angular variation of S_{11} provided that the complex refractive index is known. They also pointed to the sensitivity of S_{12} to fractal dimension and S_{34} to N almost independently of d_p.

In the studies described above it was tacitly assumed that all the primary particles were of the same size. An important question to be asked surrounds the possibility that the particles and agglomerates both have a range of sizes and what effect this may have. A detailed discussion of this has been given in the review by Sorensen (2001). Earlier, Sorensen and Wang (1999) examined agglomerates with large qR_g and looked at the effect of polydispersity on the constant in $S(q) \approx C(qR_\mathrm{g})^{-D_\mathrm{f}}$. Ideally $C = 1$, but polydispersity can have significant effects. Various equations have been proposed for this large size region and these authors explored which are the most suitable. C is dependent on the choice of cut-off function: The sharper the cut-off, the smaller the value of C. Thus it is required to find the most suitable cut-off function, and previous work has suggested that for polysdisperse aggregates a gaussian function is best. This suggests that $C = 1.0 \pm 0.05$ for D_f in the range 1.7 to 2.1. From RGD theory the authors find that

$$S_\mathrm{eff} = \begin{cases} 1 & qR_\mathrm{g,z} \ll 1 \\ C\dfrac{M_1}{M_2}\left(\dfrac{M_{2+2/D_\mathrm{f}}}{M_2}\right)^{D_\mathrm{f}/2} (qR_\mathrm{g,z})^{-D_\mathrm{f}} & qR_\mathrm{g,z} \gg 1 \end{cases}$$

where M_n is the nth moment of the distribution

$$M_\mathrm{i} = \int N^\mathrm{i} n(N)\,\mathrm{d}N$$

N is the number of primary particles in the aggregate and $n(N)$ is the number distribution function. $R_\mathrm{g,z}$ is an average of R_g weighted by the second moment of the distribution. They performed experiments on two aerosols: TiO_2 ($D_\mathrm{f} = 1.7$) and polystyrene ($D_\mathrm{f} = 2.15$). Defining

$$C_\mathrm{M} = \frac{M_1}{M_2}\left(\frac{M_{2+2/D_\mathrm{f}}}{M_2}\right)^{D_\mathrm{f}/2}$$

they found C_{M} in the range 1.53 to 1.71 for TiO_2 and in the range 2.6 to 3.6 for polystyrene. There is evidence that C_{M} increases as the width of the size distribution increases.

For chain-like aggregates with less than 20 primary particles having size parameter less than 40 and refractive index in the range 1.8 to 2.2, Charalampopoulos and Shu (2002) found that polydispersity of the primary particle size is more important than that of the number of particles per aggregate. The assumption of monodispersity tends to underestimate the real and imaginary components of the refractive index and the number of particles in the aggregate. If the standard deviation of the distribution is greater than 0.1 the effects of polydispersity must be included in any inversion procedure. The effects of polydispersity of number can be neglected if the standard deviation of this distribution is less than 0.6, otherwise the assumption of monodispersity will underestimate the real component of the refractive index but overestimate the imaginary part.

The models used in the RGD-FA calculations normally assume that the individual primary particles are just touching. However, micrographs of soot suggest that there is overlap. This is probably caused by particles colliding and fresh soot growing over the resulting combination. Brasil *et al.* (2001) looked at this and allowed for overlapping by means of a penetration coefficient.

$$C_{\mathrm{p}} = (d_{\mathrm{p}} - d_{ij})/d_{\mathrm{p}}$$

where d_{p} is the primary particle size and d_{ij} is the distance between two touching particles. If $C_{\mathrm{p}} = 0$ the primary particles are in point contact whereas $C_{\mathrm{p}} = 1$ indicates total sintering; i.e., every couple of neighbours are merged into a single particle. As a result of their modelling they suggest a fractal prefractor given by

$$K = 1.3 \exp(2.2C_{\mathrm{p}})$$

Markel and Shalaev (2001) also deal with overlapping by proposing a renormalisation procedure that retains the radius of rotation and the total volume. This takes the form

$$\begin{aligned} d'_{\mathrm{p}} &= d_{\mathrm{p}}(\xi/2)^{D_{\mathrm{f}}/(3-D_{\mathrm{f}})} \\ N' &= N(2/\xi)^{3D_{\mathrm{f}}/(3-D_{\mathrm{f}})} \\ l' &= \xi d_{\mathrm{p}} \end{aligned}$$

where l' is the distance between particle centres. ξ is an impact parameter equivalent to $C_{\mathrm{p}} + 1$ in the above, so that $1 < \xi < 2$. Calculations suggest that the best value for ξ in real clusters is between 1.61 and 1.69. With these changes the authors claim that the coupled dipole method can be used as normal.

Elongated particles in a flowing fluid with velocity gradients will have a tendency to align in the flow (Cerf and Scheraga, 1952). Studies on the scattering by aligned aggregates have been made by Botet and Rannou (2003), using a cluster–cluster model and the coupled dipole method. The results were averaged over 128 different generated aggregates. The influence of alignment is to introduce optical form anisotropy. For small aggregates the anisotropy was very

pronounced, but it vanished in the limit of large aggregates. The polarisation falls off because it arises from interactive scattering between the dipoles. Only dipoles within a distance of about 30 monomer radii can interact. For larger aggregates there are a number of such zones which are random with respect to each other, thus resulting in isotropy.

It is a tacit assumption of the RGD-FA that the primary particles are small enough to be in the Rayleigh scattering range. If they are not, then Mie theory may have to be used. Lambert *et al.* (2000) and Thill *et al.* (2000) discuss some of the consequences of this, including the need to allow for multiple scattering within the aggregate. They propose a mean field approach to deal with this involving an equivalent refractive index.

As mentioned above, in the early stages of the flame the primary particles have not had sufficient time to form agglomerates. In this case, methods are required for measurements on individual very small particles. In principle the easiest method from a theoretical point of view is Rayleigh scattering, but here the scattering polar diagram is independent of size. It is then necessary to infer the size from a combination of absolute scattered intensity (with its attendant problems) with an extinction measurement (van de Hulst, 1957).

An alternative method is dynamic light scattering, which is synonymous with photon correlation spectroscopy. Essentially this determines the Doppler frequency shifts associated with the random motion of the particles. In turn this is a function of the diffusion coefficient and the size. Since the frequency shift is due to a mechanical process, the method has the advantage that it is independent of refractive index. Lack of knowledge of this parameter is a problem for a number of optical particle sizing methods.

Usually the frequency shifts are not measured directly but are implied through their influence on the autocorrelation function. This has been briefly reviewed by Jones (1993, 1999). The correlation function takes the form

$$S(\tau) \propto \exp\left(-2q^2 D\tau - v^2\tau^2/w_0^2\right)$$

where τ is the time delay and D is the diffusion coefficient. The second term in the brackets is due to the Doppler ambiguity caused by the finite transit time across the laser beam of width w_0 by a particle with velocity v. For particles suspended in a gas, Lamprecht *et al.* (1999) suggest that

$$D = \frac{3}{8\rho a^2}\left(\frac{mk_\mathrm{b}T}{2\pi}\right)^{1/2}$$

provided that the particles are not too large. Here a is the hydrodynamic radius, ρ is the gas density, m is the average mass, k_b is Boltzmann's constant and T is the temperature. For larger particles when the concentration is not too high the Cunningham equation

$$D = \frac{k_\mathrm{b}T}{6\pi\eta a}\left(1 + \frac{L}{a}\left[\alpha + \beta\exp\left(-\frac{\gamma a}{L}\right)\right]\right)$$

may be used, where η is the gas viscosity, L is the mean free path and $\alpha = 0.864$, $\beta = 0.29$, $\gamma = 1.25$. When L approaches zero, this equation reduces to the Stokes–Einstein formula.

Cecere *et al.* (2003) used dynamic light scattering to measure the size distribution of nanoparticles produced in the non-sooting zone of ethylene/air premixed flames. The particle sizes range from 2 to 30 nm. Also, by combining *ex situ* results and the *in situ* scattering and extinction measurements in the ultraviolet, the complex refractive index of the nanoparticles was determined. The sizes obtained from DLS were independent of refractive index, and the refractive index was obtained from the ratio between extinction and vertical–vertical scattering.

However, they assumed that the real part of the refractive index was known from previous work, and obtained for the imaginary part 0.09.

Recently, Kroner *et al.* (2003) have compared static and dynamic light scattering and concluded that static scattering is better as it does not rely on *a priori* knowledge about the flame from diffusion measurements. They note that the derivation of the Stokes–Einstein formula from the basic dynamical equations of viscous flow depends on the following assumptions and comment on their applicability.

(1) Incompressibility of the medium: the compressibility of the medium starts to have effects only at velocities comparable to the speed of sound in the medium.
(2) Infinite extent of the medium: the conditions of infinite extent are never observed in practice.
(3) Very small rate of movement: Stokes law is only valid for low Reynolds numbers. (The errors are proportional to Re: At $Re = 0.1$ the difference is about 1.7%.)
(4) Constant rate of movement: this is valid for laminar flow, but not for turbulent.
(5) Rigidity of the particles: soot particles are not flexible.
(6) Absence of slipping at the particles surface: the Stokes–Einstein-relation requires that there is no velocity step at the surface of the sphere, a thin layer of medium at the surface must be fixed to the particle.

Not all of them are perfectly fulfilled, and requirement (6) is the most severe. It is not valid for measurements in gaseous media, and the Stokes–Einstein equation must be expanded by the Cunningham coefficient. They conclude that, because of all the uncertainties associated with the dynamic method, Guinier plots (as in RGD-FA) are preferable for the determination of the radius of gyration.

A method of sizing for small absorbing particles that has received considerable attention of late is laser-induced incandescence (LII). The concept here is that the absorption of a pulse of radiation from a high power laser causes heating of the particles and thermal emission. The properties are deduced from the temporal profile of the emission, and, in particular, after the pulse the rate

of cooling is observed. This rate is inversely proportional to the mass of the particles and thus the size may be obtained. The concept originated with Melton (1984), and a recent mathematical model has been given by Michelsen (2003). The first measurements based on the temporal profile appear to be due to Will *et al.* (1995). The method has become a widely used diagnostic for the investigation of soot in combustion systems, ranging from fundamental burners to practical devices such as diesel engines.

Useful comments on the method have been given by Axelsson *et al.* (2000) and Witze *et al.* (2001). Unique features of the technique are its apparent simplicity and excellent sensitivity, estimated to be better than one part per trillion ($2\,\mu m\,m^{-3}$) (Wainner *et al.*, 1999). Studies have shown good agreement between the LII signal and soot volume fraction in flames and combustion exhausts.

Witze *et al.* (2001) comment that a number of conditions need to be satisfied for the detected LII signal to be proportional to the soot volume fraction.

(1) The probed soot should consist of single or loosely aggregated primary particles that are small compared to the wavelengths of the laser excitation and the collected LII signal (such that absorption and emission occur in the Rayleigh limit).
(2) The peak particle temperatures reached during the laser pulse are relatively insensitive to the particle diameter.
(3) The soot particle mass evaporation is either negligible or largely independent of particle diameter.
(4) The detected LII signal is dominated by thermal emission occurring during laser excitation or shortly thereafter, so that size-dependent conductance cooling does not influence the signal.

Some information supporting the validity of (1) has been obtained by transmission electron microscopy grid sampling and analysis of soot in various environments, and some data demonstrating the necessity of (4) have been reported. However, little information has been gathered relative to (2) and (3).

Because the temperatures achieved by the particles can be very high (as much as 4000 to 4500 K) evaporation can be a serious problem. Also, laser ablation of soot particles can cause apparent plateaux in the signals. Signal integration times and data collection starting times are important variables. Starting measurements after the end of the laser pulse is used to eliminate problems of scattered light and fluorescence by polycyclic aromatic species. However, this slightly biases the result towards slower cooling larger particles. This can be minimised by the use of short detection times (25–100 ns). A long wave cut-off filter may be used to eliminate C_2 fluorescence from the LII signal, though a laser wavelength can be chosen to avoid this fluorescence: 532 nm or 1.06 μm are common. The choice of detection wavelength is more complicated. Long wavelengths make detection less sensitive to particle size, but short wavelengths reduce interference from flame emission.

Lehre *et al.* (2003a, 2003b) made studies on sooting flames with known properties with the specific aim of improving the mathematical model of the process.

They note that it is well established that heat loss due to radiation is a second-order effect in LII models. Further, at temperatures below 3300 K particle–gas heat transfer is the dominant cooling process. At later times after the laser pulse and during LII experiments with low laser power densities, soot evaporation can be neglected.

Measurements by Witze *et al.* (2001) suggested that there might be problems due to convective losses and thermal annealing (graphitisation). Significant evaporation loss occurs for incident power densities above $0.2\,\mathrm{J\,cm^{-2}}$.

Axelsson *et al.* (2000) combined LII with scattering-extinction measurements. Fig. 9.12 compares results by the two techniques. There is good agreement up to about 12 mm above the burner, but then the two methods drift apart. Scattering-extinction suggests that the particles continue to grow, but LII implies that the sizes tend to become constant. The authors comment that problems with scattering-extinction include variation of refractive index and polydispersity. LII can have problems with input values to the mathematical model, changes in morphology and evaporation. However, they conclude that the major differences above 15 mm are due to aggregation.

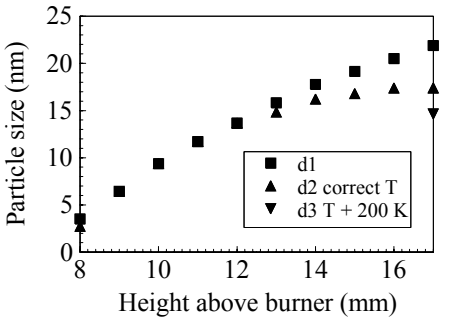

Fig. 9.12. Particle size at various heights above a burner (after Axelsson *et al.*, 2000). d1 is measured using a scattering-extinction method, while d2 and d3 are obtained using LII. The flame temperatures were measured using coherent anti-Stokes Raman spectroscopy (CARS). The point d3 illustrates the influence of varying the temperature on the LII result.

The possibility of measuring polydispersity using time resolved LII has been explored by Dankers and Leipertz (2004), using a method based on deviations from the exponential in regions where the heat loss is governed by conduction. The deviation is due to the fact that small particles have faster temperature decay than larger ones.

Snelling *et al.* (2004) deliberately kept laser power densities low to restrict soot particle temperatures to below 3500 K so that complications due to vaporisation could be avoided. To further ensure this, soot particle temperatures were measured by optical three-wavelength pyrometry. Particle sizes were obtained by sampling and electron microscopy. The fractal nature of the aggregates was

allowed for by modifying the heat transfer model by using an effective projected area equivalent diameter given by

$$d_{\mathrm{a}} = \left(\frac{N}{K}\right)^{1/2D_{\mathrm{f}}} d_{\mathrm{p}}$$

where K and D_{f} are the area pre-factor and fractal dimension. From their results they found $E(m) = 0.395$ without dispersion and 0.42 with linear dispersion, which are somewhat higher than previous authors. For example, Krishnan *et al.* (2000) reported $E(m)$ to be in the range 0.24 to 0.28 across the visible spectrum, broadly in agreement with other published values.

Another interesting technique that may prove very sensitive at low particle volume fractions is cavity ringdown (CRD) (O'Keefe and Deacon, 1988). In this a laser pulse is launched into a cavity formed by two mirrors that contains a cloud of absorbing particles. The distance between the mirrors is large in comparison to the pulse length, so that the pulse may be considered to travel back and forth many times leaking a little intensity every time it hits a mirror. On each pass there is some loss of intensity due to scattering and absorption, the consequence of which is that the pulse decays in time in a manner determined by the extinction coefficient of the particles. The CRD technique measures a characteristic exponential decay of the signal, a reference being obtained in the absence of the flame. The soot volume fraction, f_{v}, is obtained from the decay rate with the flame on, given by

$$\frac{k_{\mathrm{ext}} f_{\mathrm{v}} L}{\lambda} = \left(\frac{1}{c\tau} - 1 + R\right)$$

where $K_{\mathrm{ext}} = k_{\mathrm{ext}} f_{\mathrm{v}}/\lambda$ and l is the spacing between the cavity mirrors of reflectivity R. L is the path length in the flame, c is the speed of light and τ is the time constant of the exponential decay.

A discussion of some aspects of CRD has been given by van der Wal and Ticich (1999), who were interested in its use for the calibration of LII, which is strongly dependent on experimental conditions and details of the mathematical model. Commonly used calibration methods include extinction measurement and gravimetric sampling, but these are not effective at low soot volume fractions. Potentially CRD can measure down to one part in 10^9. Also, in CRD the laser power densities are much less than those observed to cause soot evaporation: typically $0.25\,\mathrm{J\,cm^{-2}}$ at 532 nm and $5\,\mathrm{J\,cm^{-2}}$ at 1.06 μm. Another advantage of CRD is that it yields integration over path length directly. A disadvantage is that it will not give spatially resolved results, though it gives good spatial resolution in two dimensions. It suffers similar problems to LII in the presence of scattering by large aggregates and fluorescence.

Moreau *et al.* (2004) combined LII and ringdown spectroscopy to examine soot and fluorescence of polyaromatic hydrocarbons (PAH). At 1.064 μm there is no PAH fluorescence, whereas at 532 nm both exist. They were able measure soot volume fractions down to 5 ppb.

Finally, it was noted above in passing that multicolour methods were employed to measure soot temperatures. The radiative emission by particles depends upon the emissivity of the cloud and the temperature. To determine these two unknowns, Hottel and Broughton (1932) devised a technique in which the radiation was measured at two wavelengths. Since that time the method has been widely used in a variety of ways. For two recent studies, the reader is referred to Jenkins and Hanson (2001) and Cignoli *et al.* (2001). The former authors compared absorption and emission at two wavelengths 830 and 1300 nm. The sources were modulated diode lasers. Using their method they reduced the error compared to normal two-colour pyrometry from ±50 K to ±20 K. The method is most suitable for soot volume fractions greater than 10^{-7}. Cignoli *et al.* (2001) imaged a flame onto a CCD camera at two wavelengths and were able to produce two-dimensional images of the temperature field.

9.3 Liquid fuel sprays and pulverised fuel (PF)

Both liquid and solid fuels (coal) are commonly burned in the form of small drops or particles. This is to increase the surface per unit mass, and, so, the evaporation and burning rates. For liquids, it is needed to understand the atomisation process and to follow the behaviour of the spray as a function of time and space. To this end, it is necessary to measure drop sizes and concentration (for evaporation and combustion rates) and velocity (for mass throughput). The spatial distribution of the drops is also important, as this will influence the way in which the fuel vapour mixes with available oxidant.

Among the practical problems that may be encountered are high concentration and particle shape. The former will influence whether a light beam can penetrate the spray, and can result in multiple and interactive scattering. Shape is a factor because most instruments assume that the particles are spherical. Also, the shape of the drops may affect the combustion process.

Optically the drops in a spray or PF cloud are mostly medium to large in size. This fact influences the techniques that can be used. The two most common are methods based on laser diffraction and those based on laser Doppler anemometry (LDA). A powerful version of the latter is phase Doppler anemometry (PDA).

The simple principle behind the diffraction method lies in the Airy equation

$$\sin\theta = \frac{1.22\lambda}{d}$$

where d is the particle diameter and θ is the angle of the first minimum in the diffraction pattern. There has been an extensive literature on this technique, including direct inversion to find the size distribution, the use of Mie theory to avoid error due to the diffraction approximation, the influence of shape and refractive index and the limits to particle concentration and corrections for multiple scattering. Several commercial instruments are available that make use of this fundamentally simple concept. A brief review was given by Jones (1993) with a later update (Jones, 1999).

There are two important limits to diffraction particle sizing. The method essentially assumes single scattering and so there is an upper limit to concentration before multiple scattering sets in. This is usually thought to be for transmissivities of the spray of less than 50%. Also, diffraction is an integral method and requires a minimum number of particles to achieve a sensible result for the size distribution. This is usually thought to be the concentration below which the transmissivity of the spray is more than 90%. Otherwise, integration over a long time may yield a result but this is not always satisfactory.

A number of studies have been conducted on ways to deal with high concentrations. Examples include the work of Cao *et al.* (1991) who divided the scattering volume into a series of thin, single scattering slices and calculated the progress of light through the system. They claimed to be able to extend the applicability of the diffraction method down to transmissivities of the order of 10%. Hirleman (1988) used a statistical approach to predict small angle scattering through a dense system.

More recently, Kokhanovsky and Weichert (2001a) have reviewed a number of small angle multiple scattering solutions and concluded that they are essentially all the same. Their paper provides a good discussion of the derivation of small angle solutions from the radiative transfer equation. On the basis of an azimuthally independent phase function, they obtain

$$I(\tau,\theta) = C\,\mathrm{e}^{-\tau}\int_0^1 \left[\exp\left(\frac{\tau g(z)}{2}\right) - 1\right] J_0(bz)z\,\mathrm{d}z$$

where $b = 2x\theta$, $C = \left[(2x^2)/\pi\right] I_0$, $x = \pi D/\lambda$, τ is the optical depth or turbidity and

$$g(z) = \frac{2}{\pi}\left[\arccos(z) - z(1-z^2)^{1/2}\right] \qquad z \le 1$$

For monodisperse particles they find that the size can be obtained from

$$d = \frac{\lambda h(\tau)}{2\pi\theta_0}$$

where $h(\tau) = 3.23614 + 0.0768\tau + 0.00937\tau^2$. The angle θ_0 is where the relative intensity falls to 0.5. The result is applicable for turbidities up to 6.5; that is transmissivities down to 0.15%. The authors also suggest an analytical solution for polydispersions with a gamma function size distribution. This equation has been proved experimentally by Kokhanovsky *et al.* (2001b).

Two novel diffraction instruments have been described by Gianinoni *et al.* (2003): one for very high concentrations and one for very low. In the former case the design incorporated an insertion probe with an optical configuration that made it suitable for the characterisation of high concentration particle laden flows (e.g. for pulverised coal downstream of the grinding mills) in the size range 3–300 μm. The authors noted that for high concentrations there are the following requirements:

(1) The measuring probe outer diameter must be minimised to reduce its invasiveness.

(2) The test region should be sufficiently short to prevent multiple scattering, but large enough to let the particles pass through without modifying their trajectories.
(3) The optical windows must be kept clean.

The most crucial requirement is the first one since the multi-element array sensor that collects the scattered light cannot be miniaturised without worsening its technical specifications. The minimisation of probe diameter was achieved by utilising an innovative optical scheme based on the use of a selfoc rod lens, originally developed for endoscopic applications. This lens collects the scattered light from the test region and brings it to the detector positioned far from the scattering volume outside the duct. The optical scheme of the probe is illustrated in Fig. 9.13.

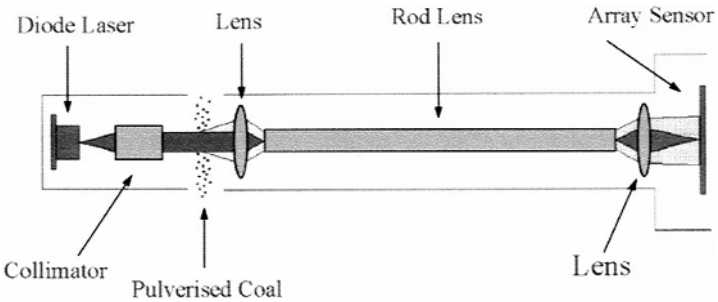

Fig. 9.13. Optical scheme of the probe developed for monitoring high concentration particle laden flows (Gianinoni *et al.*, 2003).

For low concentrations the scattered intensity is weak and particles on windows and lenses may make a significant contribution to the light received. To minimise this problem the authors reduced the number of optical components and used a converging illuminating beam focused onto a stop blade on the lens. The optical system is seen in Fig. 9.14. In this way, particles on the lens surface are no longer directly illuminated by the laser beam and do not generate undesired scattered light contributions. The authors recognise that this convergent system means that the received scattering pattern is no longer independent of the positions of the particles and discuss means of dealing with this problem. Their design enabled operation at extinction values as small as 10^{-5} in the size range 0.9–90 μm.

A deceptively simple method of measuring particle size is to measure the scattered intensity. It is expected that this will increase with volume for Rayleigh-sized particles and with area for larger particles. This is the basic principle lying behind particle counters, for example. Brief reviews of intensity measuring instruments were included in the papers by Jones (1993, 1999).

In practice, there are a number of problems with intensity measurement. First, being absolute, calibration is needed against some standard source. Also

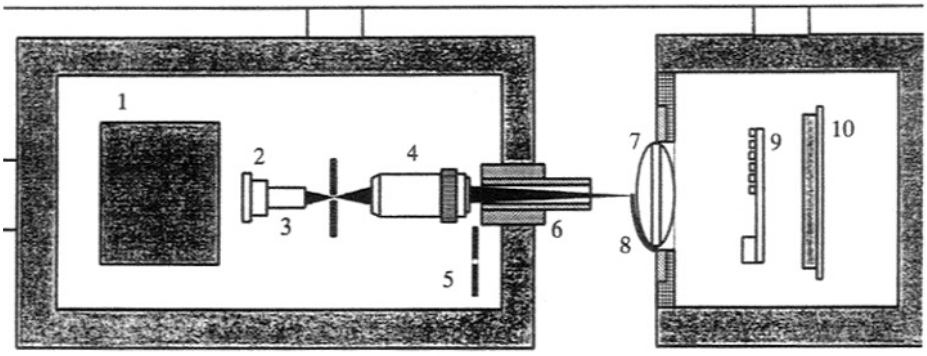

1 = Electronic box
2 = Laser Diode
3 = Selfoc Lens
4 = Microscope Objective
5 = Calibration Pin-hole
6 = Protective Pipe
7 = Collecting Lens
8 = Metallic Shell
9 = Annular Array Sensor
10 = Preamplification Card

Fig. 9.14. The measuring head of the particle sizer for low particle concentrations regimes (Gianinoni *et al.*, 2003).

the actual measured value is proportional to the strength of the illuminating light beam, so this needs constant monitoring. In combustion systems problems arise due to coating of input and output windows which changes the illumination and the transmission of the scattered light. Extinction losses along the optical paths are problematic for the same reason. Finally, there is a difficulty with the gaussian intensity profiles of laser beams since the illumination will depend upon which part of the beam the particle passes through.

With these considerations in mind it is preferable to use relative measurements as in the methods discussed below. Nonetheless, considerable effort has been devoted to particle counting devices and work continues. For example, Umhauer *et al.* (2000) have devised an instrument to enable sizing of particles in hot gases up to 1000°C. Uniform illumination of the test space is achieved by the use of a high-pressure xenon lamp as the light source. The use of a broadband source also overcomes fluctuations in the scattered intensity due to detailed variations with size and wavelength and also minor shape effects. The instrument also features a new scattering volume definition control system obtained using two masks with square apertures projected to have images vertical to each other. Protection against heat and dust precipitation is provided by having a long working distance.

A novel method of avoiding the problems associated with the gaussian profile by making use of it has been proposed by Castagner and Jones (2004). In this technique a prism was used to divide the incident beam into two parallel

gaussian beams with orthogonal polarisations. The amplitudes of the two intensities and the relative delay between them are indicative of the particle direction and velocity. Having obtained the direction of travel of a particle, its size can then obtained from the scattered intensity using Mie theory and a calibration with particles of known size. A main advantage of the method is its simplicity and lack of need of alignment. One difficulty with the method arose with non-spherical particles that cause cross-polarisation in the scattered light. This led to cross-talk between the two measured intensities. To avoid this, it was suggested that the same technique might be employed using two wavelengths instead of polarisations.

The use of LDA for particle sizing began with the papers by Farmer (1972, 1974) and Fristrom *et al.* (1973). It was recognised that an obstacle with circular cross-section traversing the interference pattern formed by two crossed laser beams would generate scattered light that oscillated in time. The frequency of this oscillation would give the velocity of the particle. However, the visibility of this signal varied depending upon the particle size and became zero for certain specific sizes. Various authors pursued this method, but it was found to suffer a number of disadvantages. The most significant of these was there are a series of zeros and the size measurement was not unique. Eventually the technique was supplanted by phase Doppler anemometry (PDA).

PDA was proposed by Durst and Zaré (1975) and came into prominence following the work of Bachalo and Houser (1984) and Saffman *et al.* (1984). In this technique the oscillatory signal is measured at a number (most usually three) of closely spaced angles, normally at about 30° (forward) or 150° (backward) out of the plane formed by the two laser beams. The phase difference between the observed oscillations is then found to have a linear dependence on particle size. Multiple angles are used to overcome the problem distinguishing phase changes greater than 2π and, thus, increase the dynamic range, typically 0.5 to 3000 μm at concentrations up to 10^{12} particles per cubic metre.

A possible way of eliminating the phase uncertainty and the need for a third detector was suggested by Onofri *et al.* (2002) in which they use multiple laser beams producing a range of spatial frequencies in the test space. To eliminate complexity of the resulting fringes the authors restricted their experiments to two overlapping fringe patterns between which interference was suppressed. This was achieved either by introducing an additional path length into one beam pair that was greater than the coherence length, or by cross-polarising the two beam pairs relative to each other.

The diffraction method makes a measurement over a volume containing the scatterers and results in a spatial average. However, PDA is a particle counting method and yields a temporal average. Thus, determination of velocity is also necessary to correct the measured size distribution. In addition, the accuracy of the measured distribution depends upon collecting a sufficient number of measurements to be statistically significant. This will be of particular importance in low concentration flows, as pointed out by Widmann *et al.* (2001a). It is then necessary to compromise between collecting a large number of samples for adequate statistics and practical data acquisition times. They investigated

the effect of insufficient sample statistics on the calculated probe area, and the resultant uncertainty in the volume flux measurement. From a range of experimental results they were able to propose corrections that resulted in statistically significant improvements.

A further problem is that there can be a trajectory error. This is because the effective size of the gaussian test space grows as the particle size increases. At the outer limits of the test space the low illumination is compensated by the higher scattered intensity. This problem is discussed, for example, by Xu and Tropea (1994), Hardalupas and Taylor (1994) and Albrecht *et al.* (1996). Zaidi *et al.* (1998) found that PDA, owing to the trajectory error, consistently gave larger drop sizes compared to those measured by the diffraction technique. Other trajectory problems associated with large particles have been tackled by Tropea *et al.* (1996) who devised a dual mode PDA, which used two orthogonal PDA beam pairs to better define the test space. More recently, Aisa *et al.* (2002) discussed the application to particles with three-directional paths. They commented that accurate measurements could be achieved if an integral method of calculation over the effective probe volume and an efficient autocalibration process are employed.

Strakey *et al.* (2000) have also examined methods of reducing many of the measurement errors. In particular, they mention the use of combined phase and scattered intensity validation methods and discuss the importance of the ratios of the angular spacing of the detectors. They also note that the use of small test space volumes can greatly improve measurement reliability in dense sprays for which multiple particle occurrences in the probe volume will affect the measurement.

The shape of the test space is generally spheroidal. Thus the size of this volume will depend upon the direction of the particle's trajectory, as noted by Yu and Rasmuson (1999). They developed a mathematical description of this effect and showed it may introduce very large errors. In the case of complex 3-D flows the projected area variation leads to a direction bias in the determination of time-averaged values of the flow. They proposed a system employing three colours, two producing independent LDA test volumes and one simply acting to define the centre of the volume. They then found that errors could be made very small.

In addition to the trajectory error there is also a slit effect, which arises from the use of a slit in the receiving optics to define the length of the measuring volume. This has been discussed by Zaidi *et al.* (1998), who pointed out that this can cause great error because for particles passing along certain trajectories the corresponding length of the measuring volume can be much longer than expected.

Problems due to particle refractive index and variations in temperature in the test space have been examined by Schneider and Hirleman (1994) and Köser and Wriedt (1996). The influence of nonspherical particle shape has been investigated by Doicu *et al.* (1996), who found that for spheroids with an eccentricity of only 0.05 there would be a phase error of 5%.

A unique new design for a PDA instrument has been described by Blondel *et al.* (2001). They note that the use of PDA in industrial environments is limited by the need for two optical access points. To overcome this they describe a monoblock instrument suitable for diesel fuel sprays that will operate with only one window, and is also compact and inexpensive. They discuss three feasible configurations, each with specific advantages and limitations:

(i) Collection in the Alexander's dark band. In this case only reflected light is collected. The measurement is then insensitive to the refractive index of the particle, but the amount of collected light is the smallest among the three possible configurations. The distance between the probe volume and the lens is also the smallest: about equal to the lens diameter.
(ii) Collection of light at the rainbow angle. Here the refractive index must be known for proper processing, but the signals are the most intense among the three configurations. However, this configuration can only be used when the particle diameter is smaller than the beam diameter. The working distance is equal to about 1.5 times the lens diameter.
(iii) Far backward collection. In this situation scattering can be dominated by three contributions depending on the particle location in the control volume: externally reflected light, internally reflected light with an impact parameter close to the edge of the particle or internally reflected light with an impact parameter close to the particle centre. The authors selected this configuration, mainly because it allows the use a large working distance: about 2–3 times the lens diameter. However, it does have the disadvantage that the different scattering modes have to be discriminated.

The design of the instrument is illustrated in Fig. 9.15. The incident beams were focused by a lens of 2 cm diameter with a focal length of 60 mm. The beam waist diameter was then as small as 40 μm and the scattering angle was 165°. These values were chosen to optimise the instrument for measurements inside a car engine.

A similar scheme for making LDA measurements in the backward direction has been proposed by Tillwick *et al.* (1999). Here the single lens both transmits and receives, but the detectors are on the periphery of the lens.

Another proposal for enabling PDA measurements at a single angle has come from Yokoi *et al.* (2001). In their technique, light scattered by a moving particle is divided into two rays that are detected with different polarisation angles to transmit dominantly reflected or refracted rays. To explore the optimum polarisation condition, they numerically investigated the phase–diameter properties in relation to polarisation angles by using the geometrical optics approximation and generalised Lorenz–Mie theory. They performed experiments with polystyrene and glass particles to verify the usefulness of the proposed method. They claim to be able to size particles up to 50 μm, but the absorption along the refracted ray must be extremely low to avoid unbalanced intensities.

An interesting situation arises when the drops are much larger than the diameter of the laser beams and the test space. In this case the drop scatters two pulses as it passes – a so-called 'dual burst'. The reason for this is that there

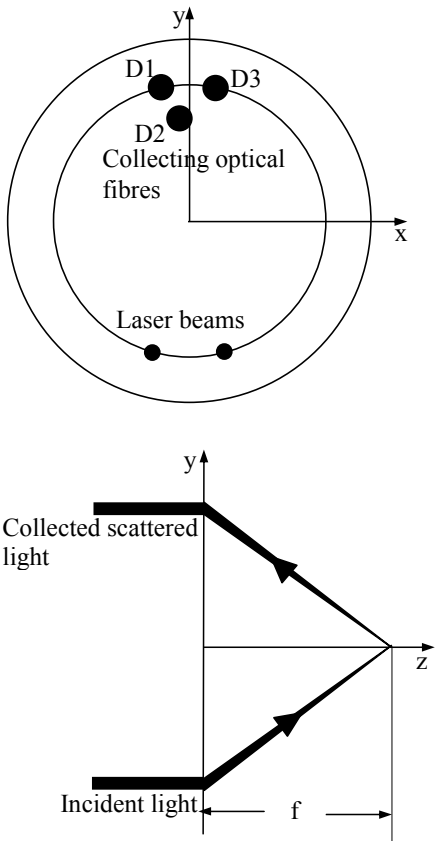

Fig. 9.15. Schematic diagram showing the geometry of the monoblock backward PDA. The top picture shows the positions of the incident laser beams and of the scattered light collecting optical fibres relative to the projecting lens. The lower picture shows the incident laser beams being brought together at the focus of the lens and of the collected scattered light originating from that point (after Blondel *et al.*, 2001).

are effectively two ray paths, as suggested by Fig. 9.16. One ray is reflected by the surface of the drop and the other is refracted through. This was originally noted by Onofri *et al.* (1996a, 1996b), who showed that, for a known particle size, the refractive index could be measured from the delay between the two pulses. Further, if the drop is absorbing the extent of absorption can be obtained from their relative heights. Thus the full complex refractive index could be obtained.

Of course, the loss of light along the refracted ray may not be caused by absorption but due to scattering or extinction loss. Thus, Onofri *et al.* (1999) proposed that the concentration of small inclusions within a drop may be determined using the dual burst technique, the properties of the main drops being obtained from reflected phase and frequency. They noted that the ratio of the refracted to the reflected signal amplitudes changes significantly with particle

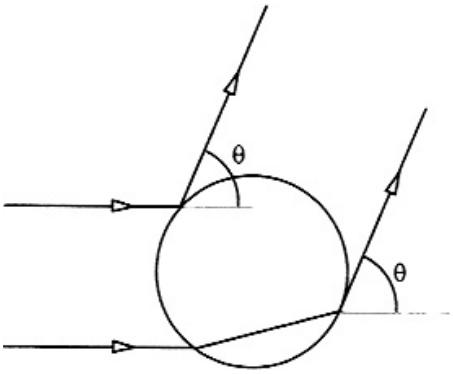

Fig. 9.16. Ray diagram illustrating the principle of the generation of two pulses by a spherical particle passing through a narrow laser beam (after Onofri *et al.*, 1996a, 1996b).

location perpendicular to the expected main direction. This is a trajectory effect that needs to be corrected for, and they discuss means of correction of this based on a gaussian laser beam. At low internal concentrations simple Beer-type transmission may be used. However, at higher concentrations multiple scattering occurs and a Monte Carlo model was applied. They performed experiments on cylindrical jets to prove the method, there being no confirmation for spherical drops.

Widmann *et al.* (2001b) have commented that the presence of burst splitting will lead to false counting of particle number and, hence, to incorrect determination of particle flux. They presented several techniques to identify the occurrence of burst splitting events, and discussed the impact of such events on the measurements. They confirmed the significance to flux measurements, but found that that the impact on size and velocity distributions was much weaker.

Damaschke *et al.* (2002a) have proposed a similar method to burst splitting to enable particle sizing in the backscatter direction at angles greater than 140°. Because of the different path lengths between the reflected and refracted rays there is a time delay between the two pulses that is proportional to the particle size. The two pulses can be separated when the particle size is rather greater than the width of the incident laser beam. Generally, the separation of the fractional signals in time will be determined by the particle size, the relative refractive index, the particle shape, and the particle velocity. Even for spheres it is necessary to know the velocity to extract the size. This can be achieved by using two laser beams in a LDA arrangement so that the velocity can be measured from the signal modulation frequency.

When it is desirable to measure the sizes of inclusions inside drops (as in a liquid containing fuel particles or soot, for example) there may be confusion caused by the presence of bubbles. Thus it is necessary to have a means to distinguish between these. Naqwi and Durst (1991) noted that the relationships between phase and size for refraction and reflection indicate that a change in

the relative refractive index around the value of unity will change the sign of the phase shift. A recent paper by Ziema *et al.* (2001) proposes a method based on this observation in which the interference fringes in the test space are made to move using Bragg cells. Separate LDA optics detect the direction of motion and velocity of the particles or bubbles. The PDA detector then monitors the sign of the phase shift.

It was mentioned above that even quite small deviations from spherical shape could result in significant errors when using PDA (Doicu *et al.*, 1996). For sizing and characterisation of solid particles, such as coal, it must be recognised that they are rarely, if ever, spherical. A modification to PDA that is capable of measuring velocity, size and shape is shadow Doppler velocimetry (SDV). In this, the particle passes through the fringes formed by two laser beams as in regular LDV and an offset detector measures the velocity from the frequency of the signal in the usual way. In addition, however, an extra lens images the particle onto a plane where a linear array detector is situated. As the shadow image of the particle crosses this detector the array gives the length of cross-section. The shape of the cross-section is then determined after the whole particle has traversed the array. A diagrammatic representation of the equipment is seen in Fig. 9.17.

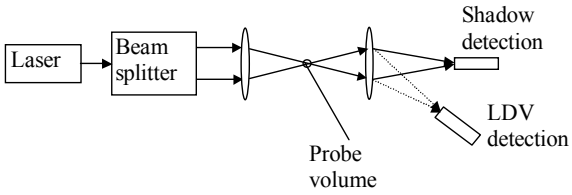

Fig. 9.17. Diagram illustrating an optical layout for shadow laser Doppler measurements (after Doicu *et al.*, 1996).

SDV was originally developed by Hardalupas *et al.* (1994) and Morikita *et al.* (1995). Concern over the influence of particles in out of focus planes on size determination (Jones *et al.*, 2002) led to a detailed analysis for two incident gaussian beams by Ren *et al.* (2003). From an extensive series of numerical computations, the behaviour of a shadow Doppler velocimeter was simulated, including the location of the image as a function of the angle between the two incident beams.

Morikita *et al.* (1995) pointed out that SDV could potentially be used to measure some extra properties of particles, such as the trajectory angle in a plane perpendicular to the optical axis. This information is especially important when precise particle shape reconstruction and flux measurements are required. However, Matsuura *et al.* (2004) state that the accuracy of the trajectory angle measurement by normal SDV is not sufficient for particles passing near the centre of the probe volume, with respect to the direction parallel to the optical axis. These authors replaced the single line array detector with two parallel

arrays of optical fibres. With a known separation of the two arrays and the measured shift of particle position can be established. In addition, stereoscopic SDV was developed by installing the arrays separately in two independent SDV optical systems. This provided stereoscopic views of the particles and enabled measurement of the trajectory angle in a plane parallel to the two laser beams, which is important for accurate particle flux estimation (Morikita *et al.*, 1997).

Rheims *et al.* (1999) proposed a system similar to shadow Doppler, except that the particle was not imaged onto the detector. In their set-up the line scan sensor covers an off-axis angular range from 30° to 60°. It is arranged in this position for two reasons: the intensity of scattered light is at maximum, and the scattered light shows distinct modulations with a clear variation with particle size. The authors provide examples of sizing homogeneous spheres and those containing emulsions.

A major advantage of LDV and PDA is that there is very good spatial resolution. However, this implies that measurements need to be made at a large number of different sites in order to obtain a spatial distribution of properties of a spray. A way to partially avoid this problem while retaining good spatial resolution in one dimension is to use a laser sheet as the illuminating source. It is then only necessary to move the sheet along one axis in the spray.

The laser sheet is formed by the use of cylindrical lenses, one of the earliest descriptions of its use being by Long *et al.* (1979). Conventional light scattering measurements can be made out of the sheet, but to obtain results over the body of a spray it has become common to observe images of the particles, either directly or by inference. Evidently the image is limited by the quality of the optical arrangement, so the method will be most suitable to particles above some minimum size.

The image of an opaque particle can be recorded directly and image analysis software can be used to retrieve the size. In principle the same is true for a transparent drop, but in that case the situation is complicated by the presence of glare spots. These arise from a reflection from the drop surface and from one refracted path through the liquid; rather in the way that dual Doppler bursts are produced for very narrow beams. These bright spots will dominate an image but can also be used for sizing. For a given scattering angle and a spherical drop the spots will always appear at the same angular position on the surface and, so, their separation is proportional to diameter. Alternatively, the image can be deliberately recorded in an out-of-focus plane. In this case the glare spots act as point sources and interfere at the detector. The fringe separation is then inversely proportional to the diameter of the drop. Fig. 9.18, after the work of Maeda *et al.* (2002), shows how the two planes may be recorded.

Burke *et al.* (2003) have described a holographic technique that is a mixture of both approaches. They state that larger droplets are best analysed at the image plane where the glare spots are recorded. However, smaller droplets are easier to analyse in the out-of-focus method and the fringe patterns are recorded. Photographic techniques allow only one of these planes to be chosen and are therefore not suitable for a range of drop sizes, whereas holography allows recording in

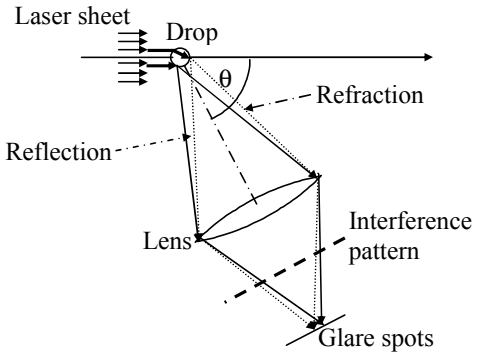

Fig. 9.18. Diagram showing the optical layout for either imaging the glare spots from a transparent sphere, or their interference pattern (after Maeda *et al.*, 2002).

depth. Unfortunately holography often suffers from low sensitivity, and in this work this problem was overcome using digital recording and analysis.

Early work on the interferometric method was reported by Roth *et al.* (1991) who gave an analysis for the angular fringe spacing on the form

$$\delta = \frac{2\lambda}{d} \frac{1}{\cos\frac{\theta}{2} + \frac{m \sin\frac{\theta}{2}}{\sqrt{m^2 + 1 - 2m\cos\frac{\theta}{2}}}}$$

where θ is the scattering angle, d is the diameter of the drop, m is the refractive index and δ is the angular fringe spacing. Later, for a scattering angle of 90°, Golombok *et al.* (1998) derived the approximate form

$$\delta \simeq \frac{2\lambda}{d} \frac{m}{m+1}$$

The full equation and the quality of the approximation were compared with Mie theory by Mounaim-Rousselle and Pajot (1999). The result is seen in Fig. 9.19. The authors claim that the significance of refractive index is small, especially at large particle sizes.

Maeda *et al.* (2002) and Kawaguchi *et al.* (2002) refer to the interferometric method as 'interferometric laser imaging for droplet sizing', or ILIDS. They note that conventional ILIDS, which observes a circular image with fringes, has difficulties at high concentration in evaluating the fringe spacing accurately owing to overlapping of the circular images. They propose a modification in which the circular images are optically compressed using cylindrical lenses. They then have the form of linear images that are horizontally defocused and vertically focused keeping the information of the location and the size of droplets. Damaschke *et al.* (2002a) derived limits on concentration to avoid overlapping images in ILIDS. They expressed their result in terms of an overlap probability coefficient as a function of number density and the parameters of the optical system.

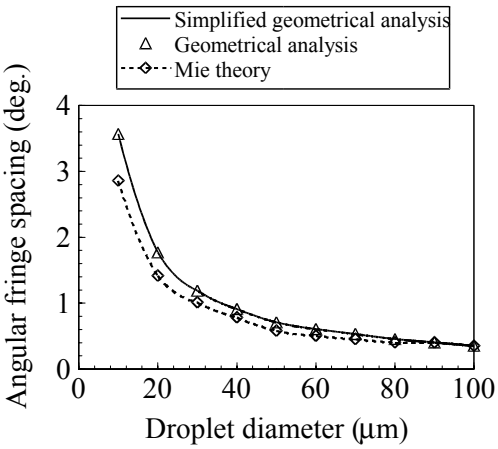

Fig. 9.19. Comparison of various calculations of the fringe spacing due to transparent drops of iso-octane as a function of drop size. The refractive index of the drops is 1.39 and the illuminating wavelength is 0.532 μm (after Mounaim-Rousselle and Pajot, 1999).

A variation on imaging was originally described by Wang and Tichenor (1991) that involved imaging particles onto a variable frequency grating. For a certain particle size roughly equal to the grating spacing the signal fell to a minimum. Velocity can also be determined. Card and Jones (2003a) developed the method by using a laser sheet that was trimmed to have a 'top hat' intensity profile both to provide uniform illumination and to restrict the depth of field. The predicted response was obtained by a Fourier analysis of a circle crossing the square wave grating, and comparison with experiment is shown in Fig. 9.20. Using this method irregular particles down to approximately 3.8 μm could be sized, the restriction being mainly due to the limited resolution of the optical system. The method was successful for certain particle types that were rough or irregular, partly absorbing or translucent. It was not successful for transparent spheres that display glare spots in the image, or other particles that produce localised regions of high brightness.

A technique showing promise is planar fluorescence imaging, which was originally suggested by Yeh *et al.* (1993). The fundamental principle behind this is that while scattered intensity is proportional to the area of the particle ($I_{\mathrm{sca}} = K_1 d^2$) the fluorescence intensity depends upon the volume ($I_{\mathrm{fl}} = K_2 d^3$). For a size distribution the average squared and cubed diameters are found and the ratio is

$$\frac{I_{\mathrm{fl}}}{I_{\mathrm{sca}}} = \frac{K_2 \overline{d^3}}{K_1 \overline{d^2}} = K_3 d_{32}$$

so that the Sauter mean diameter is measured directly. Evidently, K_1 depends upon the refractive index of the drop while K_2 is a function of the particular fluorescent dye used and its concentration. The presence of the dye may influence the refractive index of the drop if the concentration is too large, so some care

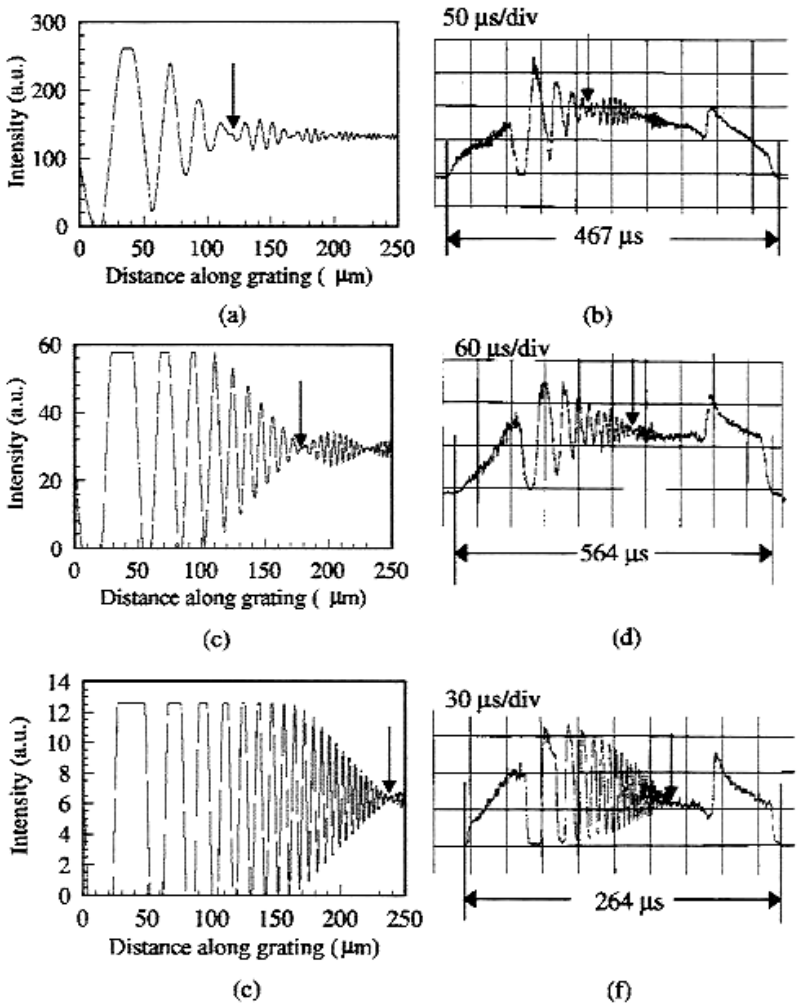

Fig. 9.20. Comparisons of theoretical predictions (a, c, e) and experiments (b, d, f) for spheres (circles) crossing a variable square wave grating. The arrows indicate the positions of the first minima (Card and Jones, 2003a).

is required. While, in principle, the functions for K_1 and K_2 can be calculated, other complications mean that calibration is required to find K_3. PDA has been used for this purpose.

Using this technique, Le Gal *et al.* (1999) produced laser sheet images of the distribution of Sauter mean diameter in a cross-section of a spray. Further, Jermy and Greenhalgh (2000) found that they could successfully measure size in a spray that was too dense for PDA. The uncertainty of the measured drop sizes was estimated at $\pm 7\%$, neglecting multiple scattering. However, it was acknowledged that multiple scattering was a large source of uncertainty.

An iterative correction scheme to allow for multiple scattering based on the Beer–Lambert law was proposed by Abu-Gharbieh *et al.* (2000). Jermy and Allen (2002) also explored the potential influence of multiple scattering using a Monte–Carlo photon transport model for transmission from the laser sheet through a half cone representing the rest of the spray. Up to 50% of the photons may be multiply scattered, but because forward scattering dominates for large particles the image is little affected. For smaller or absorbing particles the effects are more serious.

Domann and Hardalupas (2001) and Domann *et al.* (2002) have examined fluorescence intensity distributions within droplets both by geometrical optics and Mie theory. The nature of the internal structure was verified by experimental observations. A quantitative comparison of volume integrated energy results showed that for the investigated range of absorptivity Mie theory calculations lead to results that are ≈30% higher than in the geometrical optics case. Surface waves were identified as the cause for the discrepancies between the two as they cause high energy density in the rim region of the droplet images. However, the two methods gave good agreement on the general relationship between the volume and fluorescence intensity, as can be seen in Fig. 9.21. In both cases the fluorescent signal varies as $d^{2.96}$ so that the difference between Mie theory and geometrical optics can be corrected by a simple constant.

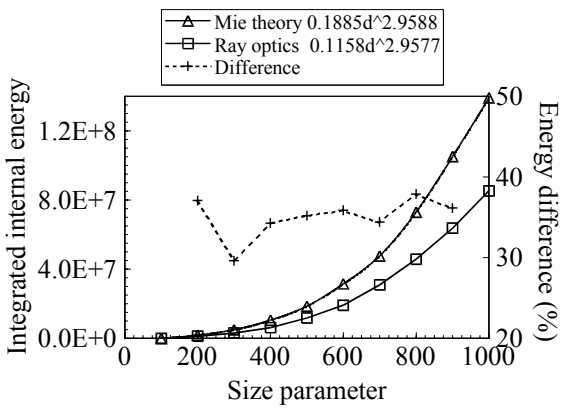

Fig. 9.21. Relationship between the volume and fluorescence intensity from a laser irradiated drop based both on Mie theory and ray optics. The refractive index of the drops is 1.333–i10^{-5} (after Domann *et al.*, 2002).

Measurements on heated water drops containing rhodamine 6G were made by Duwel *et al.* (2004) which showed that after some initial variation due to oxygen penetration, the fluorescence remained constant. This suggested that the signal is independent of drop size during evaporation and that the dye totally accumulates within the drop. In consequence, they concluded that this dye could not be used for size measurement. However, the ratio of Mie to fluorescence signal

is very sensitive to small changes in the drop surface. Potentially this could yield important information about evaporation and spray break up.

Boedec and Simoens (2001) made simultaneous measurements of velocity of droplets and ambient gas in the case of two-phase flow mixing. The basic principle of separation was to seed the ambient gas with micrometre particles and to add fluorescent dye to the liquid. The velocities were obtained using particle image velocimetry (PIV), while the fluorescence yielded the Sauter mean diameter.

An overview of fluorescence techniques in combustion systems with particular relevance to gas turbines has been provided by McDonel and Samuelsen (2000). In spray-fired systems there is a need to discriminate between phases in order to study fuel–air mixing. Numerous methods have been developed to provide information on the liquid drops, as are reviewed in this chapter. The measurement of fuel–air mixing in sprays is complicated by the need to discriminate the vapour from the liquid droplet phase. One strategy for measuring the vapour concentration in the presence of droplets is the use of light extinction. By using absorption lines at 3.39 μm for hydrocarbons in conjunction with a non-absorbing wavelength (e.g. 0.6328 μm) the vapour concentration along a line of sight can be deduced. Since the droplets scatter both wavelengths, but only the 3.39 μm wavelength is absorbed by vapour, the relative transmission of the two wavelengths yields the amount of extinction due to the presence of the vapour alone. However, there is evidence that this method may be limited to dilute sprays. Some of the practical difficulties in the application of (laser induced fluorescence) LIF in fuel–air sprays are discussed by de Sercey *et al.* (2002).

Apart from size, the refractive index of the drops in a spray is of interest. This is partly to identify the constitution of the liquid, but also to determine the temperature of the drop from the known variation of refractive index (Roth *et al.*, 1990). A technique that has been employed in this context for large drops is measurement at the rainbow angle. According to ray optics the angle at which the rainbow occurs is independent of size, which removes this variable. In addition the intensity of the scattered light is high at the rainbow. These properties make the rainbow method sound very attractive.

In reality the rainbow is only independent of size for diameters in excess of 60 μm (Massoli *et al.*, 1993). Also, a serious drawback in flames is that a temperature gradient is likely to exist within a fuel drop that will affect the rainbow position and can lead to very significant errors (Schneider *et al.*, 1993). However, Anders *et al.* (1996) using a geometric optics analysis suggested that if the surface temperature was known independently, then the rainbow could be used to measure the internal temperature gradient.

van Beeck *et al.* (2003) state that rainbow measurements on water sprays yield sizes between the normal mean and Sauter mean diameters (as measured by PDA) and temperatures correct to within a few degrees. Apart from temperature gradients, they have pointed to two other problems, namely droplet asphericity and a ripple structure that strongly perturbs the rainbow interference pattern from which one deduces the droplet's parameters. They resolved these last two difficulties by the use of global rainbow thermometry (GRT),

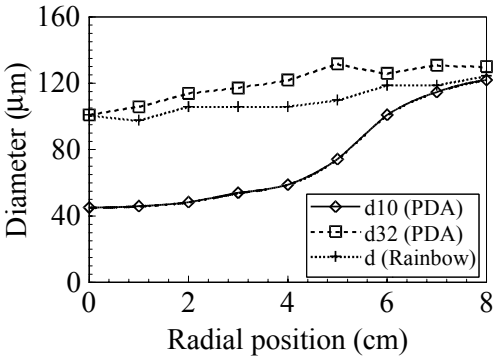

Fig. 9.22. Comparison of the mean size of drops in a fan-shaped water spray obtained from rainbow measurements with mean sizes obtained using PDA (after van Beeck *et al.*, 2003).

which was originally proposed by van Beeck *et al.* (1999). In their technique the rainbows scattered by a volume of the spray containing many drops are recorded simultaneously. In this way the high frequency ripple structures that are superimposed on the Airy fringes are averaged out owing to the size distribution, as are the effects of individual drop asphericity owing to random orientation. Their analysis is based on the angular positions of the inflection points about the main rainbow peak. Temperature is deduced from the first inflection, which is found to be very close to the geometric rainbow angle. The mean size is found from the separation between this and the second inflection. They find that the mean size obeys the equation

$$d_{\text{rainbow}} = 531.6\lambda \left(\theta_{\text{inf2}} - \theta_{\text{inf1}}\right)^{-3/2}$$

A comparison with PDA measurements is shown in Fig. 9.22.

Hom and Chigier (2002) agree that it is necessary to measure the average over many drops. For single drops less than 30 μm errors in measured water temperature can be almost ±18.8°C at 50°C and ±8.3°C for ethanol at any temperature. For larger particles this is reduced to ±5.7°C for water at 50°C and ±2.5°C for ethanol at any temperature. van Beeck *et al.* (2001) found that the temperature derivation from inflection points appears to be independent of spray dispersion, and reported preliminary measurements in a heated water spray. The accuracy of the temperature measurement by global rainbow thermometry was also shown to be a few degrees Celsius.

The potential for the use of the rainbow for absorption spectroscopy was explored by Card and Jones (2003b). By using a CCD camera and a xenon lamp light source, two-dimensional records were made of intensity against angle and wavelength for water sprays containing food dyes. The absorbance (A) is defined by $I = I_0 10^{-A}$ where I is the transmitted intensity and I_0 is the intensity in the absence of absorption. Provided that $m_2 \ll m_1$, where m_1 and m_2 are the real

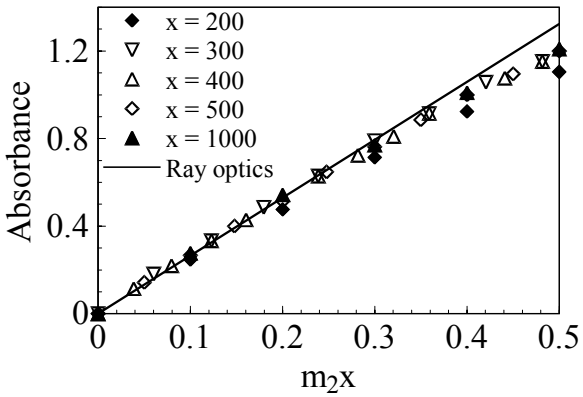

Fig. 9.23. Comparison between the ray optics prediction of absorbance at the rainbow and Mie theory for a range of size parameters, with $m_1 = 1.33$ (after Card and Jones, 2003b).

and imaginary parts of the complex refractive index, geometric optics analysis gives

$$A = \frac{16}{2.303 m_1} \sqrt{\frac{m_1^2 - 1}{3}} m_2 x$$

which is a simple linear function of the size parameter (x) and m_2. Comparisons with Mie theory, as in Fig. 9.23, show that the response is linear for $m_2 x < 0.3$. Drop sizes were estimated from the separation of the first and second rainbow peaks. Qualitatively the agreement between the theoretical predictions and the observed spectra was excellent. Quantitatively recovered values of m_2 were reasonable, though there were some discrepancies that were yet to be explained and accurate sizing is a crucial factor.

Some considerations for the future of spray diagnostics have been reviewed by Bachalo (2000).

In the combustion of coal the size and flux of particles is important, but so is their nature. As coal burns away it will form chars and ash. The latter is a particularly important product because it is non-combustible, is produced in large quantities, can have very significant effects on radiative heat transfer and causes slagging of furnace surfaces. Thus ash production needs to be monitored. Its composition is also important. If it contains too much unburned carbon this is a sign of poor combustion efficiency. Further, ash is either sold for the manufacture of concrete or is buried. In both cases the carbon content has important consequences.

An optical method for measuring the mass fraction of carbon in fly-ash was developed by Ouazzane *et al.* (2002). In this technique the particle cloud is illuminated with a polarised laser beam, but owing to the irregular shape of the particles the scattered light is partially depolarised. The extent of depolarisation depends upon the absorptivity of the particle. If the absorptivity is more then the depolarisation is less, because less light can penetrate, thus reducing the internal

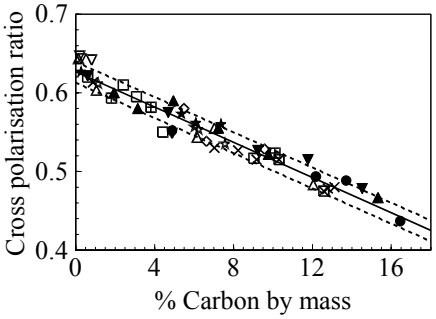

Fig. 9.24. Measurements of the residual carbon in fly ash from a range of coals by means of the cross-polarisation ratio in scattered light. The solid line is a linear least squares fit to the data, and the broken lines are plus and minus one standard deviation (after Ouazzane *et al.*, 2002).

reflections. Measurements on ashes from a wide range of coals demonstrated that there was a linear relationship between depolarisation and carbon mass fraction, as seen in Fig. 9.24.

9.4 Numerical inversion

There is a very large body of literature on the theory of direct inversion of light scattering data to yield particle size distribution. This is really beyond the scope of this chapter, especially as there is a whole journal (*Inverse Problems*) devoted to the subject. However, for the benefit of readers who may wish to pursue the subject, some of the more recent studies are referenced here.

A brief review emphasising biological particles has been provided by Popovici *et al.* (1999). They suggest that for quasi-monodisperse systems the Phillips–Twomey method is probably best, but for true polydisperse systems they preferred a combined Chahine–linear programming method.

The problem of overcoming the difficulties due to weak signals in noise and multiple scattering in dynamic light scattering systems has been studied by Buttgereit *et al.* (2001). Two scattering experiments are performed simultaneously in a three-dimensional geometry in such a way that the two scattering vectors and scattering volumes are the same, but the corresponding wave vectors do not coincide. Correlation measurements are then made at various points in the scattering pattern. Ruf *et al.* (2000) also consider noise in DLS experiments.

Inversion of diffraction measurements as in the Malvern analyser with semicircular photo-detectors is discussed by Wang *et al.* (2001). Their method begins with a guess at the size distribution represented as an N-dimensional point. The next guess is the projection of this point onto a hyperplane defined by the energy received by the next ring on the detector. The solution is represented by the point where all the hyperplanes intersect. A number of iterations of this method may

be required, but it always converges. A cut-off is determined simply by when the log of the residual error falls below a certain value. They claim that the method is stable and reliable and has good performance in the presence of noise.

A number of studies consider genetic or evolutionary programming to invert multi-wavelength extinction spectra. The method described by Lienert *et al.* (2001) searches for lognormal size distribution parameters whose calculated extinctions best fit the data. They show that, even in the case of a single lognormal distribution, many different distributions can fit the same set of extinction data unless the misfit is reduced below typical measurement error levels. In the case of a bimodal distribution, they find many dissimilar size distributions that fit the data to within 1% at six wavelengths. To recover the original bimodal distribution satisfactorily, they found that extinctions at 10 wavelengths must be fitted to within 0.5%. Li and Wilkinson (2001) discuss the retrieval of size distribution both for known and unknown refractive indices. Ye *et al.* (1999a, 1999b) conclude that genetic algorithms are superior to Monte Carlo inversion methods. Hodgson (2001) applied genetic algorithms to multimodal distributions of spheres, and Hodgson (2000) extended the technique to the determination the complex refractive index as well as size.

Li *et al.* (2004) examined light scattering by irregular particles based on the modified Wentzel–Kramers–Brillouin (WKB) and equisphere (EPS) methods and their potential to address the inverse-scattering problem by means of a spectral analysis of the total scattering cross-section of arbitrarily shaped particles. They concluded that, while EPS may be slightly better for some shapes, the modified WKB is better overall. An advantage of the two approximations is that they can easily be linearised for inversion schemes.

An inversion scheme for chain-like aggregates has been given by Shu and Charalampopoulos (2000b). The method entails the selection of suitable scattering quantities and their optimal measurement angles. The authors describe a rigorous interactive theory for chains of particles and stress the importance of correct orientation averaging.

A popular area for study is the application of neural networks to inversion. While these techniques take a long time to train, they are very rapid otherwise. Among the studies in this area are those by Wang *et al.* (1999) and Li *et al.* (2002)

Other methods include adaptive numerical filtering (Hespel and Delfour, 2000) and analytical inversion of the anomalous diffraction approximation (Franssens *et al.*, 2000)

9.5 Inclusions

In many situations there exist liquid drops containing solid particles or smaller immiscible drops. The combustion of slurries and emulsified fuels has received some attention, but one of the main areas of concern is the presence of inclusions in atmospheric aerosol. The latter may be particulates of soot, ash (either from

combustion or volcanic sources), soil or sand. The nature of these aerosols has influence on radiative transfer in the atmosphere and, thus, on climate.

Some prospects for the measurement of inclusions have been mentioned above. For optically large particles there are two glare spots, one from direct reflection from the surface and one from internal refraction. The ratio of these two intensities can be used to indicate the internal extinction losses. It has been proposed that the dual burst PDA method can be used for the same purpose, and proposals were made to discriminate between bubbles and solid particles (Naqwi and Durst, 1991; Onofri *et al.*, 1999; Ziema *et al.*, 2001).

Possible methods to measure the size of the host drop and the concentration of the inclusions based on polar diagrams have been suggested by Wriedt and Schuh (2002). Light scattering simulations showed significant changes in the scattered intensity distribution for drops with different inclusion concentrations, as can be seen in Fig. 9.25. Their evaluation reduced to only two parameters, namely angular fringe spacing and the slope in the angular scattering domain 30–70°. The fringe spacing can be used to find the size of the host particle for concentrations below 1%.

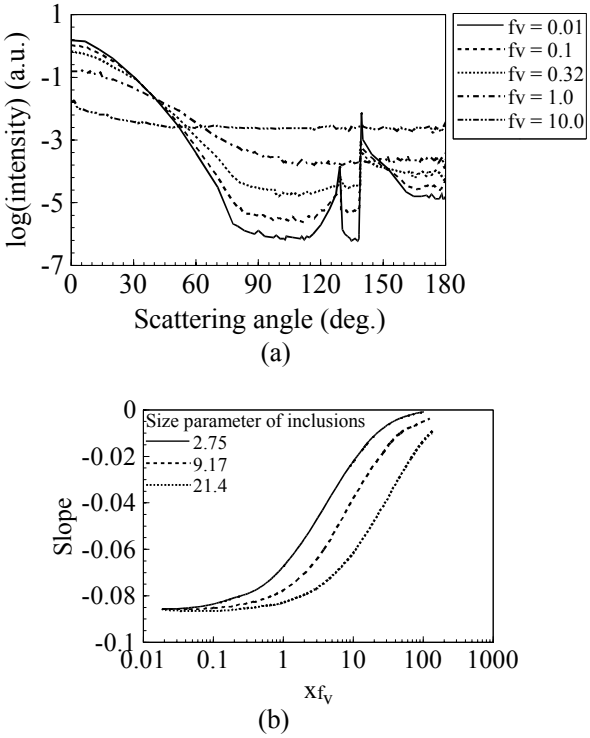

Fig. 9.25. Influence of the presence of inclusions on light scattering by drops. (a) Polar diagram as a function of volume fraction. $x_{\text{host}} = 460$, $x_{\text{inc}} = 2.75$, $m_{\text{host}} = 1.334$, $m_{\text{inc}} = 1.6$. (b) Slope of the scattered intensity in the angular range 30° to 70° for $280 < x_{\text{host}} < 1670$ (after Wriedt and Schuh, 2002).

For diagnostic and radiative transfer purposes the important parameters are the polar diagram (phase function), albedo and turbidity. For complicated compound materials a simple approach has been to derive an equivalent refractive index and perform the calculations using Mie theory. There are a number of models, perhaps the most common being the Maxwell–Garnett and Bruggeman equations.

The simple Maxwell–Garnett theory assumes that the inclusions are vanishingly small. Lakhtia and Vikram (1993) have proposed an equation that allows for finite particle size and volume fraction

$$m_{\mathrm{eq}} = m_{\mathrm{host}} \sqrt{\frac{1 + \dfrac{2\alpha f_{\mathrm{v}}}{3}}{1 - \dfrac{\alpha f_{\mathrm{v}}}{3}}}$$

where

$$\alpha = \frac{(m_{\mathrm{inc}}/m_{\mathrm{host}})^2 - 1}{1 - \left[(m_{\mathrm{inc}}/m_{\mathrm{host}})^2 - 1\right]\left[\frac{2}{3}(1 - im_{\mathrm{host}}x)\mathrm{e}^{ikm_{\mathrm{host}}x} - 1\right]}$$

Subscripts 'host' and 'inc' refer to the surrounding medium and the inclusions respectively. The authors claim that this equation is applicable for $|m_j x| \leq \pi/5$ where j is either 'host' or 'inc', and for $0 \leq f_{\mathrm{v}} \leq 0.2$.

An approximate formula based on the geometrical optics approximation was developed by Sharma and Jones (2000) for scattering by a sphere with highly absorbing randomly distributed inclusions. It was assumed that the rays propagated unperturbed in the weakly absorbing host medium, but on hitting an inclusion they were completely absorbed. In this model the real part of the equivalent refractive index is the same as that of the host medium, but the imaginary component becomes

$$m_{2,\mathrm{eq}} = \frac{3f_{\mathrm{v}}}{8x} + (1 - f_{\mathrm{v}})m_2$$

The equation was compared for dispersions of coal in water against calculations using a program developed by Mishchenko and Macke (1997) based on a Monte Carlo approach. This demonstrated that the approximation would be useful for predicting the absorption efficiency, asymmetry parameter and albedo of the sphere, as suggested by Fig. 9.26.

In a later study (Sharma and Jones, 2003) the approximation was extended to allow for absorption in the host medium together with an empirical term that allowed for finite particle size. Here

$$m_{2,\mathrm{eq}} = \frac{3f_{\mathrm{v}}}{8x} + \frac{1}{25f_{\mathrm{v}}(1 + x)}(1 - f_{\mathrm{v}})m_2$$

Doicu and Wriedt (2001) performed more rigorous calculations for the equivalent refractive index of a sphere with spherical inclusions using a recursive T-matrix method. They calculated angular scattering and then used least squares to compare the results with scattering by a homogeneous sphere with equivalent refractive index. Some comparisons with the approximate formula of Sharma and

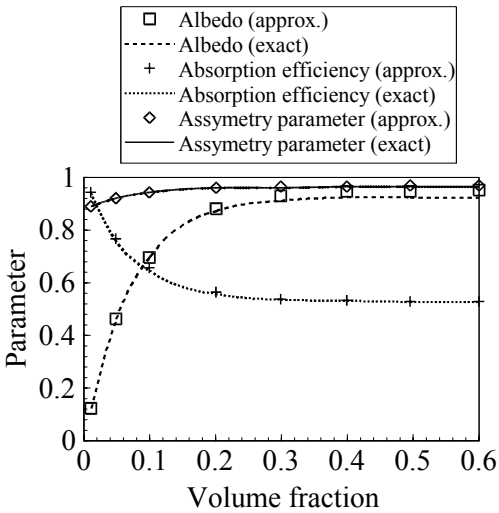

Fig. 9.26. Comparison of the albedo, absorption efficiency and asymmetry parameter for water drops containing absorbing inclusions between the approximate theory of Sharma and Jones (2000) and the exact theory of Mishchenko and Macke (1997). $d_{\text{host}} = 100\,\mu\text{m}$, $d_{\text{inc}} = 10\,\mu\text{m}$, $\lambda = 1\,\mu\text{m}$, $m_{\text{inc}} = 1.7\text{–i}0.04$ (after Sharma and Jones, 2000).

Table 9.2. Equivalent refractive index for different volume fractions (after Doicu and Wriedt, 2001). The parameters used in the calculation were $x_{\text{host}} = 500$, $x_{\text{inc}} = 25$, $m_{\text{host}} = 1.33$ and $m_{\text{inc}} = 1.28\text{–i}0.04$.

Volume fraction of inclusions	0.025	0.05	0.075	0.1
Equivalent refractive index	1.34–i0.000385	1.35–i0.000765	1.35–i0.00112	1.35–i0.00138
Refractive index from approximate formula	1.33–i0.000375	1.33–i0.000750	1.33–i0.00112	1.33–i0.00150

Jones (2000) are seen in Table 9.2. They concluded that the equivalent refractive index method is most accurate when the inclusions and the volume concentration are small and the difference between the two refractive indices is also small. At larger values the fit is much poorer and this questions the existence of a suitable solution.

The case of agglomerated soot in water was tackled by Markel and Shalaev (1999). One of their main conclusions was that the absorption of the agglomerates is enhanced. They defined the enhancement factor (G) as the ratio of the absorption cross section of carbon particles inside the water droplet and in vacuum. Fig. 9.27 shows the enhancement factor against fractal dimension. G is of the order 16 for $D_{\text{f}} = 1.8$. Markel (2002) also found that enhancement

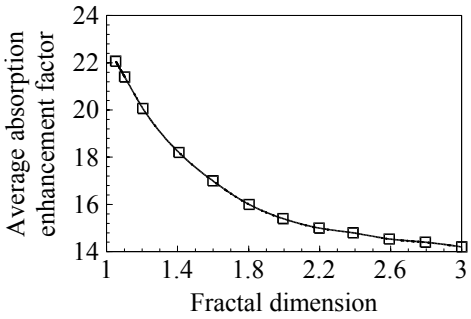

Fig. 9.27. Average enhancement of absorption due to soot in water drops ($10 < x_{\text{host}} < 1000$) as a function of the fractal dimension of the soot aggregates (after Markel and Shalaev, 1999).

factors are mostly of the order 10, but can be in excess of 10 000 at scattering resonances.

9.6 Conclusions

The literature on light scattering, even when restricted to the years after 1999, is very extensive. This chapter has concentrated on experimental methods of relevance to studies in combustion. Thus much of the recent experimental work has been omitted, and all of the theoretical studies. Even so, it can be seen from this restricted review that the field remains very active and lively.

It is probably true that the simple measurement of the size of homogeneous spheres has been very well covered over the years, and a number of excellent commercial instruments are available. As far as these spheres are concerned the remaining problems relate to measurements in difficult circumstances. Combustion is a case in point, since it presents hostile environments of high temperatures (and often high pressures) in fast-flowing dusty gases. Also, in industrial combustors such as furnaces, turbines and internal combustion engines optical access is limited.

Beyond homogeneous spheres the field remains open and active. The areas that have been covered in this chapter have included heterogeneous spheres. This relates to mixed fuels such as coal–water slurries and oil–water emulsions, and to atmospheric aerosols containing inclusions. Beyond that there remains the whole field of nonspherical particles, including the chain agglomerates that are such a feature of studies on soot and nanoparticles. In addition, there is the question of characterising particles through their refractive index and composition, examples being the measurement of temperature and quantification of residual carbon in fly-ash.

An important aspect of combustion is control because of its implications to efficiency and emissions, and thus to the environment. This has not been covered in this chapter, but evidently optical techniques play an important role.

For further information, the review by Docquier and Candel (2002) may be consulted. It gives a general review of control techniques, including a discussion of sensors.

In summary, therefore, light scattering is still an active and evolving field of study. Numerous exciting developments may be expected in the years to come.

9.7 Symbols

A	Absorbance
a	Radius of particle
a_{p}	Radius of primary particle
c	Speed of light *in vacuo*
D	Diffusion coefficient
D_{f}	Fractal dimension
d	Diameter of particle
d_{a}	Projected area equivalent diameter
d_{ij}	Distance between touching particles in an agglomerate
d_{p}	Diameter of primary particle
d_{10}	Mean diameter
d_{32}	Sauter mean diameter
$F(q)$	Scattering function for individual particles
f_{v}	Volume fraction
G	Enhancement factor
I	Intensity
I_0	Incident intensity
I_{HH}	Horizontal polarisation scattered and incident
I_{HV}	Horizontal polarisation scattered and vertical incident
I_{VH}	Vertical polarisation scattered and horizontal incident
I_{VV}	Vertical polarisation scattered and incident
K	Premultiplier in fractal description of agglomerates
K_{ext}	Extinction coefficient
$k = 2\pi/\lambda$	Wavenumber
k_{b}	Boltzmann's constant
L	Path length
l	Cavity mirror spacing
$m = m_1 - im_2$	Complex refractive index
m_{eq}	Equivalent refractive index
N	Number of particles
$\overline{N}$	Average number of particles in agglomerate
PF	Pulverised fuel
R_{g}	Radius of gyration
q	Amplitude of scattering wave vector
$\boldsymbol{q}$	Scattering wave vector
R	Reflectivity
Re	Reynolds number

$\boldsymbol{r}$	Position vector
S_{mn}	Elements of the scattering matrix
$S(q)$	Structure function in RGD theory
$S(\tau)$	Correlation function
T	Temperature
v	Velocity
w_0	Laser gaussian beamwidth
$x = \pi d/\lambda$	Particle size parameter
δ	Angular fringe spacing
θ	Scattering angle
λ	Wavelength
ρ	Density
τ	Time delay; time constant; turbidity

References

Abu-Gharbieh, R., Persson, J. L., Forsth, M., Rosen, A., Karlstrom, A. and Gustavsson, T. (2000) *Appl. Optics* **39** 1260–1267.

Aisa, L., Garcia, J. A., Cerecedo, L. M., Palacin, I. G. and Calvo, E. (2002) *Int. J. Multiph. Flow* **28** 301–324.

Albrecht, H. E., Borys, M. and Wenzel, M. (1996) *Part. Part. Syst. Char.* **13** 18–26.

Anders, K., Roth, N. and Frohn, A. (1996) *Part. Part. Syst. Char.* **13** 125–129.

Axelsson, B., Collin, R. and Bengtsson, P. E. (2000) *Appl. Optics* **39** 3683–3690.

Bachalo, W. D. (2000) *Atom. Sprays* **10** 439–474.

Bachalo, W. D. and Houser, M. J. (1984) *Opt. Eng.* **23** 583–590.

Berry, M. V. and Percival, I. C. (1986) *Optical Acta* **33** 577–591.

Blondel, D., Bultynck, H., Gouesbet, G. and Gréhan, G. (2001) *Part. Part. Syst. Charact.* **18** 79–90.

Boedec, T. and Simoens, S. (2001) *Exp. Fluids* **31** 506–518.

Botet, R. and Rannou, P. (2003) *J. Quant. Spectrosc. Radiat. Transf.* **79** 569–576.

Brasil, A. M., Farias, T. L. and Carvalho, M. G. (2000) *Aerosol Sci. Technol.* **33** 440–454.

Brasil, A. M., Farias, T. L., Carvalho, M. G. and Koylu, U. O. (2001) *J. Aerosol. Sci.* **32** 489–508.

Burke, J., Hess, C. F. and Kebbel, V. (2003) *Part. Part. Syst. Charact.* **20** 183–192.

Bushell, G. C., Yan, Y. D., Woodfield, D., Raper, J., Amal, R. (2002) *Adv. Colloid Interface Sci.* **95** 1–50.

Buttgereit, R., Roths, T., Honerkamp, J. and Aberle, L. B. (2001) *Phys. Rev. E* **6404** art. no. 041404.

Cao, J., Brown, D. J. and Rennie, A. G. (1991) *J. Inst Energy* **64** 26–30.

Card, J. B. A. and Jones, A. R. (2003a) *Part. Part. Syst. Charact.* **20** 259–266.

Card, J. B. A. and Jones, A. R. (2003b) *J. Phys. D-Appl. Phys.* **36** 236–243.

Castagner, J. L. and Jones, A. R. (2004) *Part. Part. Syst. Charact.* **21** 5–14.

Cecere, D., Bruno, A., Minutolo, P. and d'Alessio, A. (2003) *Synth. Met.* **139** 653–656.

Cerf, R. and Scheraga, H. A. (1952) *Chem Rev.* **51** 185–261.

Chang, H and Charalampopoulos, T. T. (1990) *Proc. Roy. Soc.* **A430** 577–591.

Charalampopoulos, T. T., Chang, H. and Stagg, B. (1989) *Fuel* **68** 1173–1179.

Charalampopoulos, T. T. and Shu, G. C. (2002) *Appl. Optics* **41** 723–733.

Charalampopoulos, T. T. and Shu, G. (2003) *Appl. Optics* **42** 3957–3969.
Cignoli, F., De Iuliis, S., Manta, V. and Zizak, G. (2001) *Appl. Optics* **40** 5370–5378.
Dalzell, W. H. and Sarofim, A. F. (1969) *ASME J. Heat Transfer* **91** 100–104.
Dankers, S. and Leipertz, A. (2004) *Appl. Optics* **43** 3726–3731.
Damaschke, N., Nobach, H. and Tropea, C. (2002a) *Exp. Fluids* **32** 143–152.
Damaschke, N., Nobach, H., Semidetnov, N. and Tropea, C. (2002b) *Appl. Optics* **41** 5713–5727.
de Sercey, G., Heikal, M., Gold, M., Begg, S., Wood, R., Awcock, G. and Laguitton, O. (2002) *Proc. Inst. Mech. Eng. Part C-J. Eng. Mech. Eng. Sci.* **216** 1017–1029.
di Stasio, S. (2000) *Appl. Phys. B-Lasers Opt.* **70** 635–643.
di Stasio, S. (2001) *J. Aerosol. Sci.* **32** 509–524.
di Stasio, S., Konstandopoulos, A. G. and Kostoglou, M. (2002a) *J. Colloid Interface Sci.* **247** 33–46.
di Stasio, S. (2002b) *J. Quant. Spectrosc. Radiat. Transf.* **73** 423–432.
Dobbins, R. A., Mulholland, G. W. and Bryner, N. P. (1994) *Atmos. Envir.* **28** 889–897.
Docquier, N. and Candel, S. (2002) *Prog. Energy Combust. Sci.* **28** 107–150.
Doicu, A., Schabel, S. and Ebert, F. (1996) *Part. Part. Syst. Char.* **13** 79–88.
Doicu, A. and Wriedt, T. (2001) *J. Opt. A-Pure Appl. Opt.* **3** 204–209.
Domann, R. and Hardalupas, Y. (2001) *Appl. Optics* **40** 3586–3597.
Domann, R., Hardalupas, Y., and Jones, A. R. (2002) *Meas. Sci. Technol.* **13** 280–291.
Durst, F. and Zaré, M. (1975) *Proc LDA Symp.*, Copenhagen, pp. 403–429.
Duwel, I., Schorr, J., Wolfrum, J. and Schulz, C. (2004) *Appl. Phys. B-Lasers Opt.* **78** 127–131.
Farias, T. L., Carvalho, M. G. and Koylu, U. O. (1995) *Trans. ASME-J. Heat Trans.* **117** 152–159.
Farias, T. L., Koylu, U. O. and Carvalho, M. G. (1996) *Appl. Optics* **35** 6560–6567.
Farmer, W. M. (1972) *Appl. Optics* **11** 2603–2612.
Farmer, W. M. (1974) *Appl. Optics* **13** 610–622.
Franssens, G., de Maziere, M. and Fonteyn, D. (2000) *Appl. Optics* **39** 4214–4231.
Fristrom, R. M., Jones, A. R., Schwar, M. J. R. and Weinberg, F. J. (1973) *Proc. 7th Faraday Symposium*, Chemical Society, London, pp. 183–197.
Gianinoni, I., Golinelli, E., Melzi, G., Musazzi, S., Perini, U. and Trespidi, F. (2003) *Opt. Lasers Eng.* **39** 141–154.
Golombok, M., Morin, V. and Mounaim-Rousselle, C. (1998) *J. Phys. D* **31** L59–L62.
Hardalupas, Y. and Taylor, A. M. K. P. (1994) *Exp. Fluids* **17** 253–258.
Hardalupas Y., Hishida K., Maeda M., Morikita H., Taylor A. M. K. P., and Whitelaw J. H. (1994) *Appl. Opt.* **33** 8417–8426.
Hespel, L. and Delfour, A. (2000) *Appl. Optics* **39** 6897–6917.
Hirleman, E. D. (1988) *Optical Particle Sizing: Theory and Practice* (G. Gouesbet and G. Grehan, eds.), Plenum Press, New York, pp. 135–146.
Hodgson, R. J. W. (2000) *J. Colloid Interface Sci.* **229** 399–406.
Hodgson, R. J. W. (2001) *J. Colloid Interface Sci.* **240** 412–418.
Hom, J. and Chigier, N. (2002) *Appl. Optics* **41** 1899–1907.
Hottel, H. C. and Broughton, F. P. (1932) *Ind. Engng. Chem. (Analyt. Edn.)* **4** 166–175.
Hottel, H. C. and Sarofim, A. F. (1967) *Radiative Transfer*, McGraw-Hill, New York.
Hu, B., Yang, B. and Koylu, U. O. (2003) *Combust. Flame* **134** 93–106.
Jenkins, T. P. and Hanson, R. K. (2001) *Combust. Flame* **126** 1669–1679.
Jermy, M. C. and Greenhalgh, D. A. (2000) *Appl. Phys. B-Lasers Opt.* **71** 703–710.
Jermy, M. C. and Allen, A. (2002) *Appl. Optics* **41** 4188–4196.

Jones, A. R. (1993) Light scattering for particle characterisation in *Instrumentation for flows with combustion* (A. M. K. P. Taylor, ed.), Academic Press, London, pp. 323–404.
Jones, A. R. (1999) *Prog. Energy Comb. Sci.* **25** 1–53.
Jones A. R., Parasram N. T. and Taylor A. M. K. P. (2002) *Meas. Sci. Technol.* **13** 317–330.
Kawaguchi, T., Akasaka, Y. and Maeda, M. (2002) *Meas. Sci. Technol.* **13** 308–316.
Kim, H. W. and Choi, M. (2003) *J. Aerosol. Sci.* **34** 1633–1645.
Kim, W., Sorensen, C. M. and Chakrabarti, A. (2004) *Langmuir* **20** 3969–3973.
Klusek, C., Manickavasagam, S. and Menguc, M. P. (2003) *J. Quant. Spectrosc. Radiat. Transf.* **79** 839–859.
Kokhanovsky, A. A. and Weichert, R. (2001a) *Appl. Optics* **40** 1507–1513.
Kokhanovsky, A. A., Weichert, R., Heuer, M. and Witt, W. (2001b) *Appl. Optics* **40** 2595–2600.
Köser, O. and Wriedt, T. (1996) *Appl. Optics* **35** 2537–2543.
Koylu, U. O. and Faeth, G. M. (1994a) *ASME J. Heat Transf.-Trans. ASME* **116** 152–159.
Koylu, U. O. and Faeth, G. M. (1994b) *ASME J. Heat Transf.-Trans. ASME* **116** 971–979.
Koylu, U. O. and Faeth, G. M. (1996) *ASME J. Heat Transf.-Trans. ASME* **118** 415–421.
Krishnan, S. S., Lin, K. C. and Faeth, G. M. (2000) *J. Heat Transf.-Trans. ASME* **122** 517–524.
Krishnan, S. S., Lin, K. C. and Faeth, G. M. (2001) *J. Heat Transf.-Trans. ASME* **123** 331–339.
Kroner, G., Fuchs, H., Tatschl, R. and Glatter, O. (2003) *Part. Part. Syst. Charact.* **20** 111–123.
Lakhtia, A. and Vikram, C. S. (1993) *Opt. Eng.* **32** 1996–1998.
Lambert, S., Thill, A., Ginestet, P., Audic, J. M. and Bottero, J. Y. (2000) *J. Colloid Interface Sci.* **228** 379–385.
Lamprecht, A., Eimer, W. and Kohse-Hoinghaus, K. (1999) *Combust. Flame* **118** 140–150.
Lee S. C. and Tien C. L. (1981) *18th Symp. on Combustion*, The Combustion Institute, pp. 1159–1166.
Le Gal, P., Farrugia, N. and Greenhalgh, D. A. (1999) *Opt. Laser Technol.* **31** 75–83.
Lehre, T., Jungfleisch, B., Suntz, R. and Bockhorn, H. (2003a) *Appl. Optics* **42** 2021–2030.
Lehre, T., Bockhorn, H., Jungfleisch, B. and Suntz, R. (2003b) *Chemosphere* **51** 1055–1061.
Li, M. Z. and Wilkinson, D. (2001) *Chem. Eng. Sci.* **56** 3045–3052.
Li, M. Z., Wilkinson, D. and Schrodl, M. (2002) *AICHE J.* **48** 2492–2498.
Li, X., Chen, Z. G., Gong, J. M., Taflove, A. and Backman, V. (2004) *Opt. Lett.* **29** 1239–1241.
Lienert, B. R., Porter, J. N. and Sharma, S. K. (2001) *Appl. Optics* **40** 3476–3482.
Long, M. B., Webber, B. F. and Chang, R. K. (1979) *Appl. Phys. Lett.* **34** 22–24.
Maeda, M., Akasaka, Y. and Kawaguchi, T. (2002) *Exp. Fluids* **33** 125–134.
Markel, V. A. and Shalaev, V. M. (1999) *J. Quant. Spectrosc. Radiat. Transf.* **63** 321–339.
Markel, V. A. and Shalaev, V. M. (2001) *J. Opt. Soc. Am. A-Opt. Image Sci. Vis.* **18** 1112–1121.

Markel, V. A. (2002) *J. Quant. Spectrosc. Radiat. Transf.* **72** 765–774.
Massoli, P., Beretta, F., d'Alessio, A. and Lazzaro, M. (1993) *Appl. Optics* **32** 3295–3301.
Matsuura, K., Komaki, M., Ueyama, K. and Hironaga, K. (2004) *Exp. Fluids* **36** 11–22.
McDonell, V. G. and Samuelsen, G. S. (2000) *Meas. Sci. Technol.* **11** 870–886.
Melton, L. A. (1984) *Appl. Opt.* **23** 2201–2208.
Menguc, M. P and Manickavasagam, S. (1998) *Int. J. Eng. Sci.* **36** 1569–1593.
Michelsen, H. A. (2003) *J. Chem. Phys.* **118** 7012–7045.
Mishchenko, M. I. and Macke, A. (1997) *J. Quant. Spectrosc. Radiat. Transfer* **57** 767–794.
Modest, A. F. (2003) *Radiative Heat Transfer*, 2nd edn., Academic Press, London.
Moreau, C. S., Therssen, E., Mercier, X., Pauwels, J. F. and Desgroux, P. (2004) *Appl. Phys. B-Lasers Opt.* **78** 485–492.
Morikita H., Hishida K. and Maeda M. (1995) *Developments in Laser Techniques and Applications to Fluid Mechanics*, Springer, Berlin, pp. 354–375.
Morikita H., Prassas I. and Taylor A. M. K. P. (1997) *Developments in Laser Techniques and Applications to Fluid Mechanics* (Adrian, R. J. *et al.*, eds), Springer, Berlin, pp. 233–258.
Mounaim-Rousselle, C. and Pajot, O. (1999) *Part. Part. Syst. Charact.* **16** 160–168.
Mulholland, G. W. and Croarkin, C. (2000) *Fire Mater.* **24** 227–230.
Mulholland, G. W. and Mountain, R. D. (1999) *Combust. Flame* **119** 56–68.
Mulholland, G. W., Johnson, E. L., Fernandez, M. G. and Shear, D. A. (2000) *Fire Mater.* **24** 231–243.
Mullins J. and Williams A. (1987) *Fuel* **66** 277–280.
Naqwi, A. and Durst, F. (1991) *Part. Part. Syst. Char.* **8** 245–258.
O'Keefe, A. and Deacon, D. A. G. (1988) *Rev. Sci. Instrum.* **59** 2544–2551.
Onofri, F., Blondel, D., Gréhan, G. and Gouesbet, G. (1996a) *Part. Part. Syst. Char.* **13** 104–111.
Onofri, F., Girasole, T., Gréhan, G., Gouesbet, G., Brenn, G., Domnik, J. and Tropea, C. (1996b) *Part. Part. Syst. Char.* **13** 112–124.
Onofri, F., Bergougnoux, L., Firpo, J. L. and Misguich-Ripault, J. (1999) *Appl. Optics* **38** 4681–4690.
Onofri, F., Lenoble, A. and Radev, S. (2002) *Appl. Optics* **41** 3590–3600.
Ouazzane, A. K., Castagner, J. L., Jones, A. R. and Ellahi, S. (2002) *Fuel* **81** 1907–1911.
Popovici, M. A., Mincu, N. and Popovici, A. (1999) *Math. Biosci.* **157** 321–344.
Pratsinis, S. E. (1998) *Prog. Energy Combust. Sci.* **24** 197–219.
Purcell, E. M. and Pennypacker, C. R. (1973) *Astrophys. J.* **186** 705–714.
Quinten, M., Friehmelt, R. and Ebert, K. F. (2001) *J. Aerosol. Sci.* **32** 63–72.
Ren, K. F., Girasole, T., Taylor, A. M. K. P., Gouesbet, G. and Grehan, G. (2003) *Opt. Commun.* **220** 269–280.
Rheims, J., Wriedt, T. and Bauckhage, K. (1999) *Meas. Sci. Technol.* **10** 68–75.
Riefler, N., di Stasio, S. and Wriedt, T. (2004) *J. Quant. Spectrosc. Radiat. Transf.* **89** 323–342.
Roth, N., Anders, K. and Frohn. A. (1990) *Proc. 2nd Inter. Conf. Optical Particle Sizing*, Arizona State University, Tempe, AZ, pp. 306–315.
Roth, N., Anders, K. and Frohn. A. (1991) *Appl. Opt.* **30** 4960–4965.
Ruf, H., Gould, B. J. and Haase, W. (2000) *Langmuir* **16** 471–480.
Saffman, M., Buchhave, P. and Tanger, H. (1984) *Laser Anemometry in Fluid Mechanics – II* (R.J. Adrian, D. F. G. Durão, F. Durst, H. Mishina and J. H. Whitelaw, eds), LADOAN, Lisbon, pp. 85–104.

Saija, R., Iati, M. A., Denti, P., Borghese, F., Giusto, A., Sindoni, O. I. (2003) *Appl. Optics* **42** 2785–2793.
Schneider, M., Hirleman, E. D., Salaheen, H., Chowdhury, D. Q. and Hill, S. C. (1993) *Proc. 3rd Inter. Conf. Optical Particle Sizing*, Keio University, Yokohama, Japan, pp. 323–326.
Schneider, M. and Hirleman, E. D. (1994) *Appl. Optics* **33** 2379–2388.
Sharma, S. K. and Jones, A. R. (2000) *J. Phys. D-Appl. Phys.* **33** 584–588.
Sharma, S. K. and Jones, A. R. (2003) *J. Quant. Spectrosc. Radiat. Transf.* **79** 1051–1060.
Shu, G. C. and Charalampopoulos, T. T. (2000a) *Appl. Optics* **39** 5827–5833.
Shu, G. C. and Charalampopoulos, T. T. (2000b) *Appl. Optics* **39** 6713–6724.
Snegirev, A. Y., Makhviladze, G. M. and Roberts, J. P. (2001) *Fire Saf. J.* **36** 73–95.
Snelling, D. R., Liu, F. S., Smallwood, G. J. and Gulder, O. L. (2004) *Combust. Flame* **136** 180–190.
Sorensen, C. M. and Wang, G. M. (1999) *Phys. Rev. E* **60** 7143–7148.
Sorensen, C. M. (2001) *Aerosol Sci. Technol.* **35** 648–687.
Sorensen, C. M., Kim, W., Fry, D., Shi, D. and Chakrabarti, A. (2003) *Langmuir* **19** 7560–7563.
Stagg, B. J. and Charalampopoulos, T. T. (1993) *Combust. Flame* **94** 381–396.
Strakey, P. A., Talley, D. G., Sankar, S. V. and Bachalo, W. D. (2000) *Appl. Optics* **39** 3875–3886.
Thill, A., Lambert, S., Moustier, S., Ginestet, P., Audic, J. M. and Bottero, J. Y. (2000) *J. Colloid Interface Sci.* **228** 386–392.
Tian, K., Liu, F. S., Thomson, K. A., Snelling, D. R., Smallwood, G. J., Wang, D. S. (2004) *Combust. Flame* **138** 195–198.
Tillwick, J., Uhlenwinkel, V. and Bauckhage, K. (1999) *Int. J. Heat Fluid Flow* **20** 530–537.
Tropea, C., Xu, T. H., Onofri, F., Gréhan, G., Hangen, P. and Stieglmeier, M. (1996) *Part. Part. Syst. Char.* **13** 165–170.
Umhauer, H., Berbner, S. and Hemmer, G. (2000) *Part. Part. Syst. Charact.* **17** 3–15.
Vaglieco, B. M., Beretta, F. and d'Alessio, A. (1990) *Comb. Flame* **79** 259–271.
van Beeck, J. P. A. J., Giannoulis, D., Zimmer, L. and Riethmuller, M. L. (1999) *Opt. Lett.* **24** 1696–1698.
van Beeck, J. P. A. J., Zimmer, L. and Riethmuller, M. L. (2001) *Part. Part. Syst. Charact.* **18** 196–204.
van Beeck, J. P. A. J., Grosges, T. and De Giorgi, M. G. (2003) *Appl. Optics* **42** 4016–4022.
van de Hulst, H. C. (1957) *Light Scattering by Small Particles*, Chapman and Hall, London.
van der Wal, R. L. and Ticich, T. M. (1999) *Appl. Optics* **38** 1444–1451.
Van-Hulle, P., Weill, M. E., Talbaut, M. and Coppalle, A. (2002a) *Part. Part. Syst. Charact.* **19** 47–57.
Van-Hulle, P., Talbaut, M., Weill, M., Coppalle, A. (2002b) *Meas. Sci. Technol.* **13** 375–382.
Wainner, R. T., Seitzman, J. M. and Martin, S. R. (1999) *AIAA J.* **37** 738–743.
Wang, G. M. and Sorensen, C. M. (2002) *Appl. Optics* **41** 4645–4651.
Wang, J. C. F. and Tichenor, D. A. (1991) *Appl. Opt.* **20**, 1367–1373.
Wang, J. P., Xie, S. Z., Zhang, Y. M. and Li, W. (2001) *Appl. Optics* **40** 3937–3945.
Wang, Z., Ulanowski, Z. and Kaye, P. H. (1999) *Neural Comput. Appl.* **8** 177–186.

Wentzel, M., Gorzawski, H., Naumann, K. H., Saathoff, H., and Weinbruch, S. (2003) *J. Aerosol. Sci.* **34** 1347–1370.
Widmann, J. F., Presser, C. and Leigh, S. D. (2001) *Atom. Sprays* **11** 711–733.
Widmann, J. F., Presser, C. and Leigh, S. D. (2001) *Meas. Sci. Technol.* **12** 1180–1190.
Widmann, J., Yang, J. C., Smith, T. J., Manzello, S. L. and Mulholland, G. W. (2003) *Combust. Flame* **134** 119–129.
Will, S., Schraml, S. and Leipertz, A. (1995) *Opt. Lett.* **22** 2342–2344.
Witze, P. O., Hochgreb, S., Kayes, D., Michelsen, H. A. and Shaddix, C. R. (2001) *Appl. Optics* **40** 2443–2452.
Wooldridge, M. S. (1998) *Prog. Energy Combust. Sci.* **24**, 63–87.
Wriedt, T. and Schuh, R. (2002) *Meas. Sci. Technol.* **13** 276–279.
Wu, J.-S., Krishnan, S. S. and Faeth, G. M. (1997) *J. Heat Transf.-Trans. ASME* **119** 230–237.
Xing, Y. C., Koylu, U. O., Rosner, D. E. (1999) *Appl. Optics* **38** 2686–2697.
Xu, T. H. and Tropea, C. (1994) *Meas. Sci. Tech.* **5** 969–975.
Xu, Y. L. (1997) *Appl. Opt.* **36** 9496–9508.
Xu, Y. L., Gustafson, B. A. S. (1999) *Astrophys. J.* **513** 894–909.
Xu, Y. L., Gustafson, B. A. S. (2001) *J. Quant. Spectrosc. Radiat. Transf.* **70** 395–419.
Ye, M., Wang, S. M. and Xu, Y. Q. (1999a) *Powder Technol.* **104** 80–83.
Ye, M., Wang, S. M., Lu, Y., Hu, T., Zhu, Z. and Xu, Y. Q. (1999b) *Appl. Optics* **38** 2677–2685.
Yeh, C.-N., Kamimoto, T., Kobori, S. and Kosaka, H. (1993) *Trans. JSME* 93-0134, 308.
Yokoi, N., Aizu, Y. and Mishina, H. (2001) *Appl. Optics* **40** 1049–1064.
Yu, Z. and Rasmuson, A. C. (1999) *Exp. Fluids* **27** 189–198.
Zaidi, S. H., Altunbas, A. and Azzopardi, B. J. (1998) *Chem. Eng. J.* **71** 135–143.
Zhu, J. Y., Choi, M. Y., Mulholland, G. W. and Gritzo, L. A. (2000) *Int. J. Heat Mass Transf.* **43** 3299–3303.
Zhu, J. Y., Irrera, A., Choi, M. Y., Mulholland, G. W., Suo-Anttila, J. and Gritzo, L. A. (2004) *Int. J. Heat Mass Transf.* **47** 3643–3648.
Ziema, M., Melling, A., Brenn, G. and Durst, F. (2001) *Exp. Fluids* **30** 426–433.